



HAL
open science

Modelling dose rate to single grains of quartz in well-sorted sand samples: the dispersion arising from the presence of potassium feldspars and implications for single grain OSL dating

Guillaume Guérin, Norbert Mercier, Mayank Jain, Kristina J. Thomsen,
Andrew S. Murray

► To cite this version:

Guillaume Guérin, Norbert Mercier, Mayank Jain, Kristina J. Thomsen, Andrew S. Murray. Modelling dose rate to single grains of quartz in well-sorted sand samples: the dispersion arising from the presence of potassium feldspars and implications for single grain OSL dating. *Quaternary Geochronology*, 2015, 27, pp.52–65. 10.1016/j.quageo.2014.12.006 . hal-01743074

HAL Id: hal-01743074

<https://hal.science/hal-01743074>

Submitted on 23 Jan 2024

HAL is a multi-disciplinary open access archive for the deposit and dissemination of scientific research documents, whether they are published or not. The documents may come from teaching and research institutions in France or abroad, or from public or private research centers.

L'archive ouverte pluridisciplinaire **HAL**, est destinée au dépôt et à la diffusion de documents scientifiques de niveau recherche, publiés ou non, émanant des établissements d'enseignement et de recherche français ou étrangers, des laboratoires publics ou privés.



Modelling dose rate to single grains of quartz in well-sorted sand samples: The dispersion arising from the presence of potassium feldspars and implications for single grain OSL dating

Guerin, Guillaume; Jain, Mayank; Thomsen, Kristina Jørkov; Murray, Andrew Sean; Mercier, Norbert

Published in:
Quaternary Geochronology

Link to article, DOI:
[10.1016/j.quageo.2014.12.006](https://doi.org/10.1016/j.quageo.2014.12.006)

Publication date:
2015

Document Version
Peer reviewed version

[Link back to DTU Orbit](#)

Citation (APA):
Guerin, G., Jain, M., Thomsen, K. J., Murray, A. S., & Mercier, N. (2015). Modelling dose rate to single grains of quartz in well-sorted sand samples: The dispersion arising from the presence of potassium feldspars and implications for single grain OSL dating. *Quaternary Geochronology*, 27, 52-65.
<https://doi.org/10.1016/j.quageo.2014.12.006>

General rights

Copyright and moral rights for the publications made accessible in the public portal are retained by the authors and/or other copyright owners and it is a condition of accessing publications that users recognise and abide by the legal requirements associated with these rights.

- Users may download and print one copy of any publication from the public portal for the purpose of private study or research.
- You may not further distribute the material or use it for any profit-making activity or commercial gain
- You may freely distribute the URL identifying the publication in the public portal

If you believe that this document breaches copyright please contact us providing details, and we will remove access to the work immediately and investigate your claim.

1 Modelling dose rate to single grains of quartz in well-sorted sand samples: the dispersion arising from
2 the presence of potassium feldspars and implications for single grain OSL dating

3 Guillaume Guérin^{1,2}, Mayank Jain¹, Kristina Thomsen¹, Andrew Murray³, Norbert Mercier².

4 ¹*Center for Nuclear Technologies, Technical University of Denmark, DTU Risø Campus, DK-4000 Roskilde,*
5 *Denmark.*

6 ²*Institut de Recherche sur les Archéomatériaux, UMR 5060 CNRS - Université de Bordeaux, Centre de*
7 *Recherche en Physique Appliquée à l'Archéologie (CRP2A), Maison de l'archéologie, 33607 Pessac cedex.*

8 ³*Nordic Laboratory for Luminescence Dating, Department of Geoscience, Aarhus University, DTUNutech,*
9 *Risø Campus, DK-4000 Roskilde, Denmark.*

10

11 Corresponding author: G. Guérin (guillaume.guerin@u-bordeaux-montaigne.fr)

12

13

14 **Abstract**

15 Single grain OSL has become a widely used approach in Quaternary geochronology. However, the origins
16 of D_e distributions and the sources of variation in individual dose estimates are still poorly understood.
17 The amount of scatter in these distributions on top of the known uncertainties in measurement and
18 analysis is defined by overdispersion and this quantity is generally used for weighting individual D_e
19 values to calculate a central equivalent dose. In this study, we address the nature and amount of
20 different sources of dispersion in quartz single grain D_e estimates, by (i) using appropriate statistical
21 tools to characterize D_e populations and (ii) modelling, with a specifically designed GEANT4 code, dose
22 rate distributions arising from the presence of potassium feldspar grains in well-sorted sands. The model
23 uses Monte Carlo simulations of beta emissions and interactions in a random close packing of quartz
24 and feldspar spheres representing a sand sample. Based on the simulation results, we explain the
25 discrepancy between intrinsic and natural overdispersion values in a well-bleached sample, thus
26 validating the model. The three parameters having the most influence on dispersion in dose rate
27 distributions, and modelled in this study, appear to be grain size, potassium content and total dose rate.

28 Finally an analysis of measurement uncertainties and other sources of variations in equivalent dose
29 estimates leads us to conclude that all age models (both logged and unlogged) which include an
30 overdispersion value to weight individual D_e values rely mainly on unknown parameters; this ignorance
31 may lead to an inadvertent bias in D_e estimates. Assuming counting statistics make a small contribution
32 to dispersion (as is often the case), we suggest that in some cases it is most appropriate to use
33 unweighted averages of equivalent doses when dividing by commonly measured average dose rates.

34

35 **Keywords:** Single grain OSL; dose rate distributions; age models; overdispersion; GEANT4 simulations

36

37 **1. Introduction.**

38 Quartz Optically Stimulated Luminescence (OSL) has become a widely used tool for establishing
39 the chronology of sediment burial. The Single Aliquot Regenerative protocol (SAR: Murray and Wintle,
40 2000; 2003) allows the determination of individual equivalent dose estimates (D_e) from aliquots of
41 arbitrary number of grains, including individual grains. Equivalent dose distributions derived from single-
42 grain measurements are usually significantly dispersed, requiring some statistical treatment for their
43 analysis; the choice of this statistical treatment can have a significant effect on the accuracy of the
44 resulting OSL ages. For instance, post-depositional mixing of sediments (*e.g.*, Tribolo *et al.*, 2010) and/or
45 insufficient resetting of the OSL signal before deposition (*e.g.*, Jain *et al.*, 2004; Olley *et al.*, 2004) may
46 lead to dose distributions where the central value is not representative of the sediment burial event. In
47 single-grain equivalent dose analysis, the key concept of overdispersion (OD) is defined as the dispersion
48 of results that cannot be explained by 'within aliquot errors', *i.e.* the measured or otherwise known
49 uncertainties assigned to individual equivalent dose estimates (see Galbraith *et al.*, 1999, for an
50 introduction and discussion on its significance in OSL dating; see also Galbraith and Roberts, 2012).
51 Statistical models have been proposed to identify the D_e representative of the target event. For example
52 the Minimum Age Model (MAM, Galbraith *et al.*, 1999), the IEU (Thomsen *et al.*, 2007; Jain *et al.*, 2004)
53 and the leading edge model (Lepper, 2001), have been suggested as tools to resolve the best-bleached
54 component, and the Finite Mixture Model (FMM, Galbraith and Green, 1990; Roberts *et al.*, 2000) has
55 been suggested to identify individual dose components present in a mixture. These models require the
56 input of an estimate of OD appropriate to the sample had it been well bleached; this can be either taken
57 as a value presumed to be typical of well-bleached samples in general (*i.e.* <20 %, Jacobs *et al.*, 2008a) or

58 experimentally determined from well-bleached samples with similar characteristics to those of the
59 sample under investigation (Thomsen *et al.*, 2007).

60 However, little is known about the nature and source(s) of overdispersion in single grain D_e
61 distributions. Thomsen *et al.* (2012) have demonstrated that overdispersion is dependent on dose in
62 well-bleached samples irradiated with a known gamma dose; in two samples they found the
63 overdispersion increased as the given dose increased. In naturally irradiated samples, different beta
64 dose rates to different grains in sedimentary media are also expected to contribute to overdispersion in
65 D_e values (*e.g.*, Mayya *et al.*, 2006; Cunningham *et al.*, 2012). These different dose rates arise because
66 the range of beta particles is comparable to the size of sand grains, and to the inter-granular distance. In
67 particular, the presence of hotspots – such as potassium feldspar grains, which generally represent an
68 important source of dose rates in sands – generates skewed, wide dose rate distributions (Mayya *et al.*,
69 2006; see also Brennan, 2006, for a discussion on the effect of hotspots on alpha dose rate
70 distributions). Mayya *et al.* (2006) simulated beta dose rate distributions from individual potassium-rich
71 feldspar grains to single 200 μm grains of quartz, and they showed that the dispersion in beta dose rates
72 from potassium increases as the average potassium content (*i.e.* the number of feldspar grains) is
73 decreased. Nathan *et al.* (2003) compared experimental and simulation results, using the Monte Carlo
74 radiation transport code MCNP transport code, for different cases of heterogeneity in sedimentary
75 environments. Despite weak agreement between experimental and numerical datasets, they showed
76 that beta dose rate heterogeneity (either in the form of cold or hotspots) can influence single grain D_e
77 distributions. Cunningham *et al.* (2012) used MCNP to simulate dose rate distributions induced by NaOH
78 grains containing artificially produced, short-lived ^{24}Na to mimic the effect of potassium feldspar grains.
79 They were able to reproduce the shape of experimentally determined dose rate distributions, which can
80 be fitted with log-normal distributions, but did not manage to get quantitative agreement between
81 modelled and experimental data. Nevertheless, it is now clear that the presence of radioactive hotspots

82 induces positively skewed distributions of dose rates; conversely, the presence of coldspots such as
83 calcareous blocks in 'lumpy environments' leads to negatively skewed distributions (see Brennan *et al.*,
84 1997, for a study of gamma dose rates). These distributions are in contrast to those postulated by Jacobs
85 *et al.* (2008b) who suggested that coldspots were the explanation for the two discrete modes in their
86 dose distributions; both in view of the experimental and modelling results above, this seems unlikely
87 (see also Guérin *et al.*, 2013).

88 Despite this general understanding of the effect of hotspots in governing dose distributions, very
89 few studies have compared experimental equivalent dose with simulated dose rate distributions.
90 Recently Chauhan and Singhvi (2011) compared measured equivalent dose with modelled dose rate
91 distributions, to assess whether the measured dispersion in D_e values from multi-grain aliquots could be
92 explained solely by dose rate distributions, or if an extra-source of dispersion such as poor bleaching was
93 needed to explain the scatter in D_e measurements. However, this study was not based on single grain D_e
94 measurements and it is not clear how many sensitive grains were present per aliquot. Moreover, the
95 dispersion in D_e values was taken as the standard deviation of individual estimates, and it did not
96 account for the uncertainties on the individual D_e values. In the absence of the knowledge of the effect
97 of these uncertainties, it is difficult to interpret these results quantitatively.

98 **2. Background**

99 The purpose of this study is to study beta dose rate distributions from potassium feldspar grains
100 to single grains of quartz in sand using the radiation transport toolkit GEANT4 (Agostinelli *et al.*, 2003). In
101 particular, parameters influencing these dose rate distributions are identified and the model has been
102 tested on a well-bleached, well characterised sand sample. A statistical analysis of D_e distributions from
103 both natural and gamma dosed fractions of the sample are provided, and consequences regarding the
104 use of various published age models is discussed.

105 Since D_e estimates on individual grains have highly variable uncertainties, most OSL age models
106 apply weighting factors to calculate representative equivalent doses. Moreover, most D_e distributions
107 reported in the literature exhibit overdispersion. In the most commonly used logged age models (such
108 as for example the Central Age Model and the Minimum Age Model; Galbraith *et al.*, 1999), the same
109 relative OD (in %) is added in quadrature to individual relative D_e uncertainties, assuming multiplicative
110 error properties (*i.e.* absolute uncertainties proportional to doses); the weighted average of logged D_e
111 values (geometric mean) corresponds to the central dose. Conversely, in unlogged age models the same
112 absolute OD (in Gy) is added in quadrature to individual absolute D_e uncertainties, assuming additive
113 error properties (*i.e.* constant absolute errors); the weighted average of D_e values (arithmetic mean)
114 corresponds to the central dose. In both cases the OD parameter is added in quadrature to each dose
115 estimate in the weighted mean calculation of D_e . The choice between logged or unlogged models
116 depends on the shape of measured D_e distributions: multiplicative error properties lead to lognormal
117 distributions (and to the choice of logged age models), whereas additive error properties lead to normal
118 distributions (and to the choice of unlogged age models; for a discussion on this point, see Arnold *et al.*,
119 2009).

120 Thomsen *et al.* (2012) tried to determine whether dose distributions from uniformly gamma
121 irradiated samples were normal or lognormal: they studied D_e distributions of samples bleached in a
122 solar simulator and then delivered a homogeneous well-known gamma dose, to study the nature of
123 intrinsic overdispersion. They concluded that both logged and unlogged models provided reasonable,
124 but not perfect fits to their D_e distributions; in particular, they found no evidence for multiplicative error
125 properties in equivalent dose measurements that could justify using logged age models.

126 For this study, a sand sample from a beach-ridge from Skagen (Denmark; see Buylaert *et al.*,
127 2006; Nielsen *et al.*, 2006; Guérin *et al.*, 2012) was chosen for two reasons: firstly, because its OSL

128 properties satisfy the general criteria for acceptability of the SAR protocol (fast component, recycling,
129 recuperation, dose recovery etc.) and in this area, the average OSL ages determined with large multi-
130 grain aliquots of quartz are, for a number of sediment samples (n=20), in good agreement with
131 radiocarbon data (Nielsen *et al.*, 2006); secondly, the beta dose rate from potassium contributes a
132 significant fraction (50 %) of the total dose rate to quartz; hence it is likely that, if dose rate distributions
133 are affected by potassium and have implications regarding single-grain D_e populations, such an effect
134 will be observed in this sample. It thus is a good candidate to (i) model beta dose rate distributions from
135 potassium and (ii) experimentally characterise the implications of such modelling for analysis of
136 equivalent dose distributions. As a result, the effect of potassium feldspar grains on the dispersion of D_e
137 measurements from the natural distribution is presumed to be significant. Following Buylaert *et al.*
138 (2006), this sample will be referred to as ‘the inter-comparison sample’.

139 **3. Samples, material and methods**

140 **3.1. Sample preparation and characterization**

141 **Gamma spectrometry**

142 Sediment was homogenised by crushing and sealed in a plastic box containing ~10 g of material.
143 This sealed sample was then stored for at least three weeks to ensure radon build-up, before
144 measurement using high resolution, low background gamma spectrometry, at the IRAMAT-CRP2A in
145 Bordeaux. The potassium, uranium and thorium contents are given in **Table 1**. The corresponding dose
146 rates have been calculated using dose rate conversion factors from Guérin *et al.* (2011) and using grain-
147 size attenuation factors from Guérin *et al.* (2012). The accuracy in dose rate determination, using the
148 infinite matrix assumption, has been questioned in general – and for this sample in particular – by
149 Guérin *et al.* (2012), especially when it comes to grain-size attenuation factors for uranium and thorium.
150 However, the exact value of the attenuation factors (constants) is not critical for our study since we are

151 only interested in comparing the equivalent dose and dose rate distributions in this sample; we
152 therefore used attenuation factors for beta dose rates from uranium and thorium. The effect of
153 moisture on gamma dose rate was taken into account following Guérin and Mercier (2012), using the
154 mean grain size of the sample and using the cubic-centred packing model. For the effect of moisture on
155 beta dose rates, we used the water correction factors from Nathan and Mauz (2008) in sediments
156 containing no carbonates, which were indirectly confirmed by Guérin and Mercier (2012). Here it should
157 be noted however, that these correction factors have not been adapted to sand samples (for which the
158 geometry of energy emission and absorption has consequences on the effect of moisture on beta dose
159 rate – see Guérin et al., 2012). For the potassium feldspar extracts, the internal dose rate was calculated
160 using dose rate conversion factors for potassium (Guérin *et al.*, 2011) and the self-dose values from
161 Guérin *et al.* (2012), and assuming an internal potassium content equal to $12.5 \pm 0.5\%$ (Huntley and Baril,
162 1997). Finally, the contribution from Rb was calculated according to Readhead (2002) and Huntley and
163 Hancock (2001).

164 **Grain size analysis and element composition**

165 Grain size analysis and single grain element composition were obtained from Scanning Electron
166 Microscope (SEM) image analysis and Energy Dispersive Spectrometry (EDS), respectively. Guérin *et al.*
167 (2012) already modelled dose rates in this sample but their study focused on average dose rates to the
168 different grain-size classes. Nevertheless, the sample characteristics were taken from this previous
169 study: the grain size distribution can be found in their Fig. 1 (where the frequency corresponds to the
170 actual number of grains rather than the most commonly used mass fraction). The sample is a well-sorted
171 medium sand, with a mean grain size of $360 \mu\text{m}$ (geometric mean following Folk and Ward, 1957,
172 calculated using the GRADISTAT program, Blott and Pye, 2001; in the following, all mean grain sizes are
173 calculated accordingly). Based on EDS analysis, it is mainly (>99% by number of grains) made up of three

174 minerals: quartz (85% of the grains), potassium (7%) and sodium (8%) feldspar. Single grain EDS analysis
175 further revealed that the grain-size distribution of potassium feldspar grains is similar to that of the
176 sample taken as a whole. The potassium concentration, calculated from the abundance of potassium
177 feldspar grains, and assuming a 12.5 % K content of these feldspars (corresponding to the peak in the
178 histogram of K concentration from single grains, Fig. 2 in Guérin *et al.*, 2012) is ~1 % by mass and
179 compares very favourably with gamma spectrometry results (Table 1).

180 **Sample preparation**

181 Prior to mineral separation, the sample was wet sieved to isolate 180-250 μm sand grains. These
182 grains were then treated with HCl (10%) to remove carbonates, and with hydrogen peroxide (H_2O_2) to
183 remove organic contaminants; despite a weak reaction, both treatments were continued until no
184 further reaction was visible. Two aqueous solutions of sodium heteropolytungstates (densities 2.58 and
185 2.62 g.cm^{-3}) were used to isolate K-rich feldspar fractions ($<2.58 \text{ g.cm}^{-3}$) and quartz ($>2.62 \text{ g.cm}^{-3}$). The
186 quartz fraction was then etched with HF (40%) for 40 minutes to remove the outer portion of the grains
187 affected by alpha irradiation. After etching, any fluoride contaminants were removed by rinsing with
188 10% HCl. This fraction was then re-sieved to $>180 \mu\text{m}$ for further analysis, in particular for single grain
189 measurements; this latter step removes any $<180 \mu\text{m}$ grains resulting from the dissolution of residual
190 feldspar in the quartz-rich fraction, or of small quartz grains.

191 **3.2. Luminescence instrumentation**

192 Grains were mounted in 9 mm base-diameter stainless steel cups using silicon oil. Aliquots of ~6
193 mm in diameter were measured for quartz, at the IRAMAT-CRP2A in Bordeaux, and of ~3 mm in
194 diameter for feldspar extracts, at Risø. Luminescence measurements were made using Risø TL/OSL DA-
195 15 and DA-20 readers (Bøtter-Jensen *et al.*, 2003; 2010); for quartz multi-grain aliquots, blue (470 nm)
196 light-emitting diodes (LED) were used with 7.5 mm Hoya U-340 detection filters; for feldspar, IR diodes

197 emitting at 875 nm were used in combination with coupled Schott BG39 and Corning 7-59 detection
198 filters (transmission 320–460 nm). Each $^{90}\text{Sr}/^{90}\text{Y}$ source was calibrated during the measurement period
199 by measuring several aliquots of calibration quartz irradiated with gamma rays (4.81 Gy; hereafter
200 referred to as Risø calibration quartz) from a national secondary-standard ^{137}Cs source; this calibration
201 has been independently confirmed by Bos *et al.* (2006).

202 Single grains of quartz were measured using an automated Risø TL/OSL reader (DA 20) fitted
203 with a single grain attachment (Duller *et al.*, 1999; Bøtter-Jensen *et al.*, 2000). The grains were loaded
204 into aluminium single-grain discs; each disc contains 100 holes 300 μm in diameter and 300 μm deep, on
205 a 10x10 rectangular grid with 600 μm spacing between centres. A green laser (532 nm) was used to
206 stimulate these grains individually, with light detection through a 7.5 mm Hoya U-340 glass filter. To
207 confirm that only one grain was loaded into each hole, the single grain discs were visually inspected
208 using a microscope before measurement. Radiochromic films allowed the determination of a coefficient
209 of variation of 5.6% in dose rates to individual positions on the single-grain disc (Lapp *et al.*, 2012).
210 Correcting for this spatial variation in dose rates to single grains did not significantly change the
211 measured D_e distributions, so we used a single beta source dose rate for all grain positions.

212 **3.3. Modelling: LSD algorithm and GEANT4**

213 The model used in this study was already described in detail by Guérin *et al.* (2012) and a
214 previous version of the GEANT4 code is available in Guérin (2011). Here GEANT4 (Agostinelli *et al.*, 2003;
215 Allison *et al.*, 2006) is used to simulate the beta emission spectra from potassium feldspar grains (**Fig. 1**;
216 such grains represent 7% of the total), and to track each primary (electron) and secondary (photon and
217 electrons) particle transport individually in a random close packing of spherical grains. The random close
218 packing is based on the Lubachevski-Stillinger-Donev (LSD) algorithm (Donev *et al.*, 2005). The grain size
219 distribution of the sample was determined experimentally by SEM image analysis (sample grains were

220 thinly spread on a glass plate to ensure no grain overlap). The equivalent radius of the grains was
221 determined assuming spherical grains (by equivalent radius of a grain we mean the radius of a circle
222 whose surface would correspond to apparent, generally irregular surface of the grain). The compactness
223 of the sediment obtained by random packing of the grains, using the LSD algorithm, is 0.635; as a result,
224 the density of the medium when air fills the pore space, is calculated to be 1.68 g. cm^{-3} .

225 The sample water content, as determined experimentally, is 12% - which corresponds to a
226 sediment density of 1.88 g.cm^{-3} . To obtain the same density for the wet sediment in our Monte Carlo
227 simulations, air is replaced by uniform, 'light water' (with a density of 0.55 g.cm^{-3}) in pore spaces; this
228 leads to a calculated wet density for the simulated sediment equal to the experimental value. Here it
229 should be noted that these dry and wet sediment density values corresponding to the simulations are
230 close to 'typical' sediment densities such as those given *e.g.* by Aitken (1985, Appendix H). The low
231 density, uniformly distributed 'water' is an approximation; in practice, surface tension effects alter the
232 spatial distribution of water (density: 1 g.cm^{-3}) in the pore spaces – water forms thin layers at the
233 surface of grains and tends to accumulate where grains touch each other. Such modelling goes beyond
234 the scope of this study, however, it is difficult to say if a more realistic distribution of water would
235 significantly affect the results of the simulations. For charged particles, the stopping power (unit: $\text{cm}^2.\text{g}^{-1}$)
236 ¹⁾ determines the energy loss in the media, so for example, energy loss in $10 \mu\text{m}$ of water with a density
237 of 0.55 g.cm^{-3} is equivalent to crossing $5.5 \mu\text{m}$ of identical water but with a density of 1 g.cm^{-3} ; one can
238 ignore here $4.5 \mu\text{m}$ of air because of the negligible mass. As a result, in terms of energy loss in pore
239 space, the two scenarios are equivalent (light, uniformly distributed water, or dense, localised water and
240 air). However, some difference between the two cases will occur in terms of directional straggling; but
241 these are expected to even out on average.

242 Beta particles are emitted isotropically and their starting point is sampled homogeneously
243 within the feldspar potassium grains. For simplicity, Guérin *et al.* (2012) simulated either pure potassium
244 feldspar grains (with a K content of 14%, following stoichiometric values), or grains with zero potassium
245 content. This assumption allows simplification of the simulations; however, the continuous distribution
246 of K in the grains (cf. SEM-EDS analysis presented in Fig. 2 of Guérin *et al.*, 2012) suggests that the actual
247 potassium distribution may be somewhat less heterogeneous than in the model. Here, it should be
248 noted that: (i) the potassium content of grains having a K content less than 6% are considered as zero
249 potassium grains; this is considered acceptable since these grains represent only ~10-15 % of the total
250 potassium in the sample; (ii) SEM-EDS analyses characterise only the surface of the grains, while the
251 beta dose rate originates in the entire volume (so SEM-EDS values might not be representative of the
252 content of the grains). We also observed low but non-zero values of K content from measurement of
253 quartz grains, implying that at least some K is residing on the surface of all grains. Thus, the number of
254 feldspar grains with intermediate K values is likely to be even lower than that observed in the data,
255 suggesting that our assumed binary distribution of K should have little influence on the validity of the
256 simulation results.

257 For tracking of both photons and electrons, Penelope physics datasets were used, as they are
258 well-adapted to the simulation of low energy electromagnetic interactions (Salvat *et al.*, 2001).
259 Production cuts (*i.e.* range of secondary particles below which these secondary particles are not
260 generated) and maximum step size were set to 20 μm to ensure accurate tracking down to one tenth of
261 the diameter of the dosimeter grains of interest. In other words, the energy that would be carried away
262 by a particle with a range of less than 20 μm was assumed to deposit locally, and the interaction
263 probabilities were recalculated, by extrapolation of the provided Penelope datasets, every 20 μm along
264 the particles tracks. To mimic infinite matrix conditions, a reflection algorithm was used (Nathan, 2011;
265 Guérin *et al.*, 2012).

266 Whereas in Guérin *et al.* (2012), the dose was only recorded in the grain-size classes of interest,
267 in this study every quartz grain in the range from 180 to 250 μm in diameter is treated as an
268 independent dosimeter; this allows us to obtain beta dose rate distributions from potassium feldspar to
269 quartz grains. For each set of simulations (*i.e.* for each grain size distribution and potassium content),
270 ten different random close packing configurations were used. For each configuration, the emission and
271 tracking of 20,000,000 primary particles were simulated at the calculation centre of the French National
272 Institute of Nuclear and Particle Physics (IN2P3). The uncertainties on the different numbers given in the
273 following are obtained by taking the standard errors on individual values from the 10 different simulated
274 configurations.

275 **4. Results**

276 **4.1. Multi-grain aliquots OSL, IRSL and age control**

277 For the inter-comparison sample studied here, the quartz OSL signal is dominated by the fast
278 component. The SAR protocol (Murray and Wintle, 2000; 2003) was used with a preheat temperature of
279 200°C, held for ten seconds, and a cutheat temperature of 180°C before test dose measurements. The
280 net signal intensity used in further calculations was derived from the sum of the OSL in the first 0.8 s of
281 stimulation minus a background signal (calculated from the following 2.4 s of stimulation, *i.e.* early
282 background subtraction). Nine aliquots were first exposed to a SOL 2 solar simulator for 3 hours and
283 then given a dose of 5 Gy in the luminescence reader. The measured to given dose recovery ratio
284 (0.97 ± 0.05) showed that our SAR protocol was well-suited to measure equivalent doses for this sample.
285 21 equivalent doses were measured using multi-grain aliquots of quartz; the average recycling ratio was
286 0.99 ± 0.07 , and the resulting equivalent dose and age (4.73 ± 0.23 ka) are shown in Table 2.

287 The IRSL from ~ 3 mm aliquots of K-rich feldspars was also measured ($n=6$); the corresponding
288 equivalent dose is 6.90 ± 0.30 Gy. A g-value of 2.8 ± 0.2 %/decade was obtained from fading

289 measurements performed on the same aliquots. Using the fading correction from Huntley and Lamothe
290 (2001), the resulting age of 4.28 ± 0.27 ka is in good agreement with the quartz OSL age, which confirms
291 that the quartz OSL signal was well reset at the time of deposition (*cf.* Murray *et al.*, 2012). A post-IR
292 IRSL at 290 °C (pIR-IR₂₉₀; Thiel *et al.*, 2011) dose of 13.7 ± 0.6 Gy was obtained from six different aliquots,
293 giving an apparent age of 6.69 ± 0.36 ka. This age overestimation of ~ 2 ka is not surprising given the
294 young age of the sample since it is well-known that residual, difficult-to-bleach doses affect post-IR IRSL
295 D_e determination from young samples. It corresponds to a residual dose of ~ 6 Gy for this signal, which
296 fits within the variability of observed residual doses for well-bleached samples (*i.e.*, samples sufficiently
297 exposed to sunlight to reset the quartz OSL signal; see, *e.g.*, Buylaert *et al.*, 2011). This further indicates
298 that the quartz OSL from this sample is most likely unaffected by poor-bleaching.

299 **4.2. Single grain OSL D_e and dose rate distributions.**

300 The single grain D_e measurements were all made using the SAR protocol with a preheat at 260
301 °C for ten seconds, and a cutheat at 220 °C prior to test dose response measurement (note that thermal
302 transfer is negligible for this sample, *cf.* Nielsen *et al.*, 2006). The net signal used in D_e calculations was
303 derived from the sum of the OSL in the first 0.05 s of stimulation minus a background signal (time
304 average of the last 0.2 s; total stimulation time: 1s). Dose estimates from individual grains were
305 accepted if they passed the following rejection criteria (derived from Thomsen *et al.*, 2005; 2007; 2012):
306 an error on the first test dose signal of less than 20% and a recycling ratio consistent with unity at two
307 standard deviations. Recuperation was negligible for all samples. Note that the purity of the quartz
308 extracts was examined on multi-grain aliquots using an IR-test (IRSL/BLSL ratios < 1%; Murray *et al.*,
309 submitted).

310 Fig. 2 shows the relationship between the first ('natural') test dose signal and measured
311 equivalent dose for single grains (i) from the international calibration standard "Risø calibration quartz"

312 (batch 54, heated and then given a 4.81 Gy dose using a secondary-national standard ^{137}Cs source in
313 scatter free-geometry, Fig. 2a), (ii) from fractions of quartz from the inter-comparison sample exposed
314 to a solar simulator for three hours and then given gamma doses of respectively 1.92, 4.81 and 9.62 Gy
315 (Figs. 2b, c ,d), and (iii) from natural quartz from the inter-comparison sample (Fig. 2e).

316 **4.2.1. Single grain gamma dose distributions**

317 **Table 3** lists a number of statistical characteristics of the equivalent dose distributions of figure
318 2, and resulting D_e measurements derived using different statistical models: the Central Age Model
319 (CAM; Galbraith *et al.*, 1999), the CAM_{UL} (Arnold *et al.*, 2009) and a simple unweighted arithmetic mean;
320 where relevant, dose recovery ratios are also given; all dose recovery ratios are within 10% of unity.
321 Furthermore, they are all consistent with unity, within two standard errors (except for the 1.92 Gy dose
322 recovery test, where the CAM_{UL} gives a measured to given dose ratio equal to 0.93 ± 0.03).

323 The Risø calibration quartz and the inter-comparison sample show different average
324 luminescence intensities in response to a fixed test dose of 2.2 Gy (first test dose signal). Furthermore,
325 the average luminescence intensity of the signals induced by gamma irradiations in dose recovery
326 experiments depends on the given dose. As a consequence, the average relative uncertainties on
327 individual dose estimates vary between the different samples: 13% for the Risø calibration quartz (given
328 dose: 4.81 Gy) and 27%, 21 % and 13 % for the inter-comparison sample for given doses of 1.92, 4.81
329 and 9.62 Gy, respectively (see **Table 3**). However, the relative overdispersion (OD) values from the CAM
330 show little variation between Risø calibration quartz and the inter-comparison sample, or as a function
331 of dose for the latter (16% on average; *cf.* **Table 3**); the different OD values for the gamma dose
332 recovery experiments are statistically indistinguishable, which confirms the pattern seen by Thomsen *et*
333 *al.* (2007; 2012) in the low dose region. Similar conclusions can be drawn for the CAM_{UL} , when the
334 absolute OD (in Gy) is expressed as a fraction of the central dose. **Fig. 3** shows a standardised residual

335 analysis in the form of quantile-quantile plots (see Galbraith and Roberts, 2012, for other examples of
336 such plots and their discussion). Quantile-quantile plots can be used to visually assess the normality of
337 the distribution of residuals from the models. The standardised residuals $((d_i - \delta) / \sigma_i)$, where d_i is the i^{th}
338 measurement of dose, σ_i its associated uncertainty – *i.e.*, the quadratic sum of the analytical uncertainty
339 and the overdispersion – and δ is the central value determined with the model) are sorted and plotted
340 against the estimates expected from a normed and centred Gaussian distribution. The 1:1 line indicates
341 the expected fit to the data if residuals are normally distributed.

342 Interestingly, from **Fig. 3** it can be seen that for the gamma dose distributions, the standardised
343 residuals from both the CAM and the CAM_{UL} are consistent with a normal distribution, *i.e.* the observed
344 residuals plotted against a normal distribution fall on a 1:1 line, despite a few outliers in the tail regions.
345 In other words, it appears that the intrinsic overdispersion can be well described either by the same
346 relative or the same absolute uncertainty; this makes the choice between normal and lognormal age
347 models arbitrary at this stage.

348 **4.2.2. Dose rate distributions to single grains**

349 One of the differences between laboratory gamma dosed and the natural D_e distributions lies in
350 the different dose rates to which individual quartz grains have been exposed in sedimentary media. **Fig.**
351 **4** shows the results of the GEANT4 simulations of the single-grain beta dose rate distribution from
352 potassium feldspar grains for the inter-comparison sample. This distribution is positively skewed
353 (skewness: 1.07) and can be fitted by a lognormal distribution (red line), which is in agreement with
354 previously published work (Mayya *et al.*, 2006). The positive skewness can be understood as a result of
355 few quartz grains being close to potassium feldspar grains (high dose rate tail of the distribution),
356 whereas most quartz grains are at some distance – compared to the range of beta particles – from beta
357 radioactive sources (mode of the distribution). The distribution has a relative standard deviation of

358 31.2±1.4 %. Note that the presence of hot-spots does not lead to any distinguishable bi-modality in the
359 resulting dose rate distribution.

360 Grain to grain variations in gamma and cosmic dose rates can reasonably be assumed to be
361 negligible in this sample, given the range of these radiations (>tens of cm). We assume that there is no
362 other source of dispersion in beta dose rates to quartz grains – which is difficult to prove but supported
363 by the absence of heavy minerals such as zircons, apatites, etc. from the SEM-EDS analysis (these could
364 be potential sources of uranium and thorium). As a consequence, the relative standard deviation of the
365 total dose rates to single grains of quartz (15.6±0.7 %) is obtained by multiplying the dispersion in beta
366 dose rates from potassium by the relative contribution of this component to the total (50 %).

367 **4.2.3. Over-dispersion in the inter-comparison natural sample**

368 Equivalent doses measured for the natural portion of the inter-comparison sample are plotted
369 against natural test dose responses in **Fig. 2e**. Standardised residual analyses from the CAM and the
370 CAM_{UL} are shown in **Fig. 5**. As for the gamma dosed populations, both models provide good fits to the
371 experimental data, and the resulting equivalent doses are consistent with each other.

372 At least two contributions to the OD from the natural equivalent dose population have been
373 quantified at this stage: (i) an intrinsic OD (*i.e.* the OD resulting from the measurement protocol); in
374 other words we regard this intrinsic OD to originate from unrecognised/unquantified uncertainties
375 inherent in the measurement, rather than as so-called ‘natural variations in the OSL properties’ giving
376 rise to different true equivalent doses – cf. Galbraith et al., 2005). Our best estimate of this is
377 determined from the gamma dose recovery tests in the dose range of interest (section 4.2.1); and (ii) an
378 extrinsic OD (*i.e.* the OD resulting from all environmental factors external to the grains, such as the
379 degree of light exposure before burial and grain-to-grain variations in dose rate). In this sample, we

380 consider the extrinsic OD to be dominated by the dispersion in dose rates (section 4.2.2), since we are
381 confident that the sample was well bleached at deposition.

382 In this sample, we have determined the intrinsic OD from the CAM ($15\pm 3\%$ at ~ 5 Gy) and the
383 standard deviation in dose rates ($15.6\pm 0.7\%$); these can be summed quadratically to give a minimum
384 estimate of OD that should be observed in the natural sample, of $22\pm 3\%$. This compares very favourably
385 with the measured OD ($23\pm 2\%$); thus, it seems that the natural OD for the well-bleached inter-
386 comparison sample can be fully explained by two contributions: the intrinsic OD and the dispersion in
387 dose rates.

388 **4.3. Factors influencing the dispersion in dose rates**

389 Given that it appears that dose rate variations contribute about 50% to the total OD in our
390 sample, it is now useful to investigate the factors influencing the dispersion in dose rate to single grains.
391 This was done by varying several parameters of the GEANT4 model. Mayya *et al.* (2006) have already
392 shown the effect of average potassium concentration on dose rate distributions in sands where
393 potassium is located in potassium-rich feldspar grains: the skewness and dispersion of dose rate
394 distributions increase as the number of potassium-rich grains is decreased (relative to the number of
395 quartz grains). This can be understood by considering that the average distance between source and
396 dosimeter grains is increased as the potassium content is decreased because of a reduction in the
397 number of feldspar grains; as a result, fewer quartz grains are close to potassium sources and most are
398 at a distance from any source. Similarly, one would then also expect that the average grain size of the
399 sediments would have a similar effect on dose rate distributions: as the grain size is increased, the
400 distances between source and dosimeter grains is also increased, which should lead to more skewed
401 and more dispersed distributions.

402 Two parameters were thus varied in the simulations: firstly, the potassium content was varied
403 by changing the fraction of potassium-rich feldspar grains, while keeping the grain size distributions
404 similar for quartz and feldspar; secondly, the grain size distributions of the whole sample were
405 multiplied by different scaling factors, so that the sorting of the sediments remained untouched but the
406 simulated grain size distributions went from fine/very fine sands up to medium/coarse sands (**Fig. 6**).
407 **Fig. 7** shows frequency histograms of beta dose rate distributions to quartz grains for various grain size
408 distributions and average matrix (bulk) potassium concentrations. The relative standard deviation of
409 these distributions is plotted in **Fig. 8**, for different grain sizes, as a function of average potassium
410 content. As expected, the relative dispersion increases when the potassium content is decreased and/or
411 when the grain size is increased, up to 135 ± 19 % for a mean grain size of $637 \mu\text{m}$ with a K content of
412 0.14%.

413 We have compared our results, in terms of relative standard deviation in beta dose rates from
414 potassium feldspar, with those presented by Mayya *et al.* (2006) in their Fig. 4. For 1% potassium and a
415 unique grain size ($200 \mu\text{m}$), Mayya *et al.* (2006) found a relative standard deviation of $\sim 28\%$; for a mean
416 grain size of $255 \mu\text{m}$, we found 20% and only 9% for $149 \mu\text{m}$. It is not straightforward to understand
417 these differences, partly because the two approaches are so different (in particular, Mayya *et al.*
418 focused on determining the minimum dose due to the presence of hotspots: Morthekai, Pers. Com.),
419 and parameters may have different values. For example, the emission of beta particles in their paper is
420 considered to be point-like, whereas in the Monte Carlo simulations the initial position within the
421 emitting grains is sampled homogeneously. Straggling effects are taken into account in our Monte Carlo
422 modelling, but not in Mayya *et al.* (2006). Furthermore, in their paper the minimum distance between a
423 quartz grain and the closest hotspot – defined as the distance between the centres of the two
424 corresponding grains (Morthekai, Pers. Com.) – is 0; in other words, two grains can overlap, which is
425 physically unrealistic. This may seem to be negligible, but it most likely explains the important high dose

426 tails in their Fig. 3. b (it should be emphasized that this did not affect the minimum dose due to the
427 presence of hotspots). Finally, there is an apparent peak in the dose distributions for very low doses (cf.
428 Fig. 3a), which according to the original authors is a numerical artefact (Morthekai, Pers. Com.); this
429 could contribute to the relative standard deviation in dose rates. It is very difficult to know at this stage
430 if one or more of these factors can explain the difference between our results and those from Mayya et
431 al. (2006). Nonetheless, despite these differences, the tendencies observed when parameters are varied
432 (in particular potassium content) remain the same. Because Monte Carlo simulations have fewer
433 approximations and closely mimic nature and because we model a more representative sediment
434 matrix, we tend to believe that the results of our simulations are better representative of the deviation
435 in dose rates due to the presence of hotspots compared to the approximate analytical treatment in
436 Mayya et al. (2006).

437 It should be emphasised here that, for a given potassium content and assuming that beta dose
438 rates from potassium are the only source of grain to grain dose rate variations, the dispersion on total
439 dose rates to quartz grains will decrease as the total dose rate is increased; this is because the relative
440 contribution to dose rate from potassium is decreased. In other words, the dispersion values from **Fig. 8**
441 should always be scaled by the relative contribution of beta dose rates from potassium to the total. In a
442 comprehensive study of more than 4,000 sediment samples from various contexts and geographical
443 locations, Ankjærgaard and Murray (2007) have shown that beta dose rates account on average for
444 ~67% of the total dose rates (when working on sand-sized grains previously etched with concentrated
445 HF, *i.e.* not accounting for any alpha dose rate contribution). Moreover, for 95% of the samples, ^{40}K
446 contributed between 40 and 92 % of the total beta dose rate. In other words, the contribution to the
447 total dose rate to quartz grains from the beta dose rate derived only from potassium ranged from 27 to
448 62% in almost all cases. **Fig. 9** shows the modelled dispersion in total quartz dose rates as a function of
449 potassium content for three samples in each of which the total dose rate is fixed (at 1, 2 and 3 Gy.ka⁻¹).

450 The known likely range of potassium-derived beta dose rate contribution to the total (27 to 62%,
451 derived above) are shown as dashed lines in **Fig.9**; these indicate the likely standard deviations to be
452 expected for well-sorted sands of different mean grain sizes, for typical K concentration.

453 **5. Discussion**

454 **5.1. Typical OD for well-bleached samples**

455 Many age models (FMM, MAM, IEU) require the input of an OD value before the model can be
456 used to identify a representative dose component(s). Determining an accurate OD representative of a
457 well-bleached population is, therefore, at the heart of most single-grain studies. Sometimes, the intrinsic
458 OD determined by a dose recovery experiment is used as a minimum value (*e.g.*, Thomsen *et al.*, 2007);
459 in other studies the OD is allowed to vary between fixed values (*e.g.*, Jacobs *et al.*, 2008b).

460 The results from our Monte Carlo simulations show that a typical OD value for a well-bleached
461 sample will depend on grain size, potassium content, and total dose rate. Considering the effect of
462 potassium feldspar grains on dispersion in single-grain dose rates, there is no *a priori* limit on the OD of
463 a natural sample and certainly no typical OD for well-bleached samples. This could explain the wide
464 range of ODs observed in natural samples presumed to be well-bleached (but presumably affected by
465 beta dose rate heterogeneities, see Fig. 1 of Thomsen *et al.*, 2012, and references therein; see also, *e.g.*,
466 Jacobs, 2010; Jacobs *et al.*, 2011; 2012; 2013; Gliganic *et al.*, 2012).

467 **5.2. When to use the dose rate model**

468 It should be emphasised that the model presented here is expected to be used in cases where
469 single grain dose rates need to be simulated to disentangle different sources of OD in single grain D_e
470 measurements. In this study, the model successfully explains the discrepancy between the observed OD
471 in the natural D_e distribution and the intrinsic OD resulting from the measurement protocol, for a single

472 sample. It is difficult to predict how well it might perform on a variety of samples. Nevertheless, our
473 understanding of the processes involved allows us to be confident that dispersion in beta dose rates
474 arising from the distribution of potassium will be most important when the average grain size is in the
475 sand and gravel range (rather than silt or clay), the potassium content is low (<1%), and the total dose
476 rate is small (<1 Gy.ka⁻¹).

477 **5.3. Implications for the use of different age models**

478 Interestingly, in the literature so-called age models (*e.g.*, CAM, MAM, FMM) are actually dose
479 determination models. Very few studies focus on dose rates during burial, even fewer consider dose
480 rate distributions in the analysis of single-grain dose distributions. The simulation results presented in
481 this study raise important questions concerning how luminescence ages are calculated. In particular, it is
482 not clear how individual data should be weighted; each single grain equivalent dose estimates is not
483 measured with the same precision, and each grain has received a different unknown dose rate; thus a
484 dose distribution is not equivalent to an age distribution.

485 In the ideal case of a single 'true dose' (*i.e.*, every grain has absorbed the same dose), the central
486 dose (in this section, by central dose we mean the value most appropriate for use with an average dose
487 rate to derive an age) is commonly derived using the logged or the unlogged central age model (see
488 section 2). An alternative approach, commonly used in multi-grain analyses, is to use the unweighted
489 arithmetic mean; this approach discards analytical uncertainties on individual dose estimates on the
490 grounds that these uncertainties are trivially small compared to the variability in D_e measurements. The
491 use of this latter approach inherently implies that the main source of dispersion is unknown and is much
492 bigger than all known sources of analytical uncertainty.

493 The intrinsic dispersion in the D_e data can generally be equally well described by normal and
494 lognormal distributions. However, the dose rate distribution from potassium feldspar grains is

495 positively skewed and can only be best described by a lognormal distribution; each individual dose
496 component of this distribution is sampled in the lab as a normal or a log normal distribution. In many
497 cases dose recovery distributions can be adequately fitted using the CAM (which assumes a log normal
498 distribution); this has been demonstrated here by the Gaussian distribution of the residuals from the
499 CAM (Fig.3 – right panel), using the inter-comparison sample. Given that log normal distributions can
500 describe both the natural dispersion arising from dose rates, and the measurement induced dispersion
501 in the data, suggests that the use of logged models best represent D_e distributions in natural samples,
502 and so provide the best estimates of OD.

503 The question is how best to determine the burial dose from a distribution of single grain D_e
504 values, in the absence of the knowledge of the underlying dose rate distribution. Almost all dose rates
505 based on high resolution gamma spectrometry, Neutron Activation Analysis (NAA), beta counting or any
506 other analytical technique are arithmetic means of repeated measurements of the spatially averaged
507 radioactivity in the sample. Thus, we typically know only an average dose rate in the sample. The dose
508 distribution on the other hand is known at the single grain level and different measures of central
509 tendency can be applied to derive a representative dose. If an age is derived by dividing a geometric
510 mean D_e by an arithmetic mean dose rate, then the age is likely to be underestimated to some degree
511 (since unweighted geometric means are systematically lower than unweighted arithmetic means). For
512 example, consider a sample in which the distribution of dose rates dominates the natural dispersion.
513 Suppose this to be a well-bleached, well-behaved sample in which the uncertainty on the measurement
514 of dose is negligibly small (*e.g.*, 1%). All grains must by definition record the same age. First, consider a
515 10 ka old fine-grain sample with a uniform dose rate of 1 Gy/ka. We measure 3 grains, each with a dose
516 of 10 Gy: the average age is 10 ka and the CAM age is 10 ka with no overdispersion. Now let us consider
517 a less homogeneous (coarse grained) sample, of the same age and average dose rate, from which we
518 sample three representative grains which have experienced dose rates of 0.6, 0.9 and 1.5 Gy/ka

519 resulting in doses of 6, 9 and 15 Gy. We still observe the average dose rate (1 Gy/ka), the dose
520 distribution is positively skewed, and the individual grain ages of course remain at 10 ka; the average
521 age is 10 ka but the CAM age (using a geometric mean of D_e values) is 9.3 ka. Thus, it appears that if the
522 scatter in the measured equivalent dose distribution arises primarily as the result of grain to grain
523 variability in the dose rates (which is much larger than the intrinsic variability due to measurement), and
524 one measures an average dose rate, then it is more appropriate to use the simple mean rather than the
525 geometric mean D_e .

526 More generally, the equivalent dose derived from measured D_e distributions using any age
527 model should be as close as possible to the average of the true underlying dose rate distribution.
528 Sometimes, this will be best estimated using the CAM (or geometric mean); for instance, when all grains
529 have received the same dose and the dominant source of dose dispersion is multiplicative error
530 properties. However, in those cases where the dose rate distribution is unknown but the natural dose
531 distribution is considerably overdispersed compared to a (gamma) dose recovery experiment, it seems
532 reasonable to assume that the dominant source of dispersion is dose rate (in any case, it is unlikely to be
533 explained by multiplicative error properties, because these should be entirely accounted for by the dose
534 recovery experiments). In such cases the central dose may be best estimated by using an unweighted
535 arithmetic average; the CAM will bias the results to give an equivalent dose inappropriate to the average
536 dose rate, and so an underestimate of the age. Obviously, this approach has the drawback that one
537 gives equal weight to individual D_e values that are known with different degrees of precision.

538 To some extent, the above problem could be circumvented if a geometric mean dose rate was
539 available. However, only direct measurement of single-grain dose rate distributions would allow the
540 calculation of geometric mean dose rates; in general, such data is not obtainable experimentally. For the
541 inter-comparison sample, the geometric mean of the GEANT4 simulated single-grain beta dose rates

542 from potassium is ~5% lower than the arithmetic mean; in the absence of uncertainties on D_e
543 measurements (or if they are negligible compared to other sources of dispersion), using a geometric
544 mean to calculate a central dose (*e.g.*, CAM) together with an average dose rate would thus result in an
545 age underestimation of ~2% compared to that using the arithmetic mean for equivalent dose and dose
546 rate (since beta dose rate from potassium contributes ~50 % of the total). In a worst case scenario, the
547 difference between geometric and arithmetic means of beta dose rates from potassium could be as
548 much as 50% (based on a simulation assuming $[K] = 0.14 \%$, mean grain size of $637 \mu\text{m}$ – cf. Fig. 8). Then
549 the discrepancy arising from the division of a geometric mean equivalent dose estimate by an average
550 dose rate would result in an age underestimation of 25%. Although this effect depends on potassium
551 content, grain size and total dose rate, it should be noted that the consequence of using a geometric
552 mean is a systematic age underestimation, not a random variation about some mean. In absence of
553 modelled data such as presented in this study (or a better analytical approach), it appears that
554 arithmetic means of D_e should give us the most accurate age.

555 **5.4. A case study: the inter-comparison sample**

556 In this sub-section, we discuss in practice the choice of an appropriate analysis model for D_e
557 calculation, following the simulation results obtained for the inter-comparison sample.

558 In the natural D_e distribution of the well-bleached inter-comparison sample, three main factors
559 contribute to variations in D_e estimates, each with similar magnitudes: known measurement
560 uncertainties, an intrinsic source of scatter in single-grain doses (measurable, but of unknown origin;
561 Thomsen *et al.*, 2005; Galbraith *et al.*, 2005), and finally dose rate variations. **Fig. 10** shows the
562 relationship between the absolute (**Fig. 10a**) or relative (**Fig. 10b**) errors and individual dose estimates
563 for the gamma dose recovery distribution obtained using the inter-comparison sample. The data are
564 highly scattered, and no clear trend is observable; if anything, there may be a weak tendency for the

565 relative uncertainties to decrease with dose. Both the CAM and CAM_{UL} indicate that the data are
566 overdispersed, with a magnitude similar to the dispersion of measurement uncertainties. Finally, Fig. 10
567 (c, d) shows the same plots of uncertainty as a function of dose for the distribution of D_e estimates from
568 the natural inter-comparison sample. Again there is no unique trend, although overdispersion is
569 increased presumably due to variations in external beta dose rates. In all four cases it is difficult to
570 ascertain which age model, *i.e.* CAM, CAM_{UL} or unweighted arithmetic average, to use.

571 It is interesting to note that experimentally, for the equivalent dose populations investigated in
572 this study, the CAM-based equivalent doses are greater than CAM_{UL} results (Table 3), because – even
573 though there is no clear trend in the graphs from Fig. 10 – average relative uncertainties appear to
574 decrease slightly with increasing dose (thus placing more weight on higher dose estimates when using
575 CAM), and inversely for absolute doses (with the consequence of lowering CAM_{UL} central dose).

576 The fact that we measure non-zero intrinsic OD values tells us that we underestimate our
577 uncertainties on individual D_e estimates, possibly due to variability in grain to grain natural OSL
578 properties that is not accounted for by analytical uncertainties. When applying our GEANT4 based dose
579 rate model, the only source of systematic variation in D_e distributions that we know of – albeit only
580 through modelling – is the variation in dose rates to individual grains; it is difficult to justify using this
581 source of dispersion in the weighting of D_e estimates (as is the case when using *e.g.* the CAM), as dose
582 rate variability is independent of uncertainties of dose estimates. We may then decide to simply ignore
583 our uncertainties in central D_e estimations and calculate unweighted averages of equivalent doses. Not
584 only are the dose recovery tests satisfactory (*cf.* **Table 3**), but doing so we would also compare
585 arithmetic means of equivalent doses with arithmetic means of dose rate. In the case of the inter-
586 comparison sample, (i) the three identified sources of dispersion in D_e (analytical uncertainties, intrinsic
587 and extrinsic OD) are of comparable sizes and (ii) the intrinsic OD is reasonably well-fitted by both

588 normal and lognormal distributions of corresponding uncertainties (cf. standardised residual analyses of
589 the CAM and the CAM_{UL}); it is not surprising that all three models (including an unweighted arithmetic
590 average) give a set of consistent ages. In general, we argue that only a careful analysis of the sources of
591 dispersion can lead to an informed decision regarding the most appropriate D_e determination model on
592 a sample by sample basis.

593 Our study has not considered issues related to changes in OSL sensitivity of the grains between
594 nature and laboratory irradiations; any such changes can be a source of additional intrinsic over-
595 dispersion in D_e populations (undetected by gamma dose recovery experiments; see, *e.g.*, Stokes,
596 1994a, b; Singhvi *et al.*, 2011). But given that there is a satisfactory agreement between the observed
597 OD and the predicted OD (from intrinsic OD and beta dose rate variation), we think this sensitivity
598 change effect must be negligible. From a dose rate perspective, the presence of highly radioactive
599 minerals such as, *e.g.*, zircons will also induce additional extrinsic over-dispersion. Our Geant4 model
600 was designed to describe the effect of potassium feldspar grains on extrinsic over-dispersion, because
601 this was considered the most likely and most important source – at least for beta dose rates.
602 Nevertheless, similar models using the same architecture can be used to predict the effect of uranium
603 and thorium sources of any given geometry and size distributions.

604 **6. Conclusion**

605 We have developed a new model to quantify the effect of grain size and potassium
606 concentration (feldspar hotspots) on the grain-to-grain dose rate variations for well sorted sediments.
607 The model is successfully tested using experimental data obtained from a well characterised sediment
608 sample, and predictions are made for other sediments with similar sorting but different grain sizes and K
609 concentrations. The model provides estimates of minimum expected extrinsic overdispersion for various
610 grain size distributions, potassium contents and total dose rates. These estimates, together with an

611 analysis of over-dispersion in laboratory dose recovery data (intrinsic overdispersion), allow us to
612 investigate the sources of variability in equivalent dose measurements from individual grains in our test
613 sample. It is shown that consideration of beta dose rate variability has an important bearing on the use
614 of statistical models such as CAM, MAM, FMM, IEU, etc. for deriving the representative equivalent dose
615 that corresponds to the average dose rate estimate. Furthermore, our results imply that, for well
616 bleached samples, unweighted arithmetic mean dose together with the average dose rate may provide
617 a more accurate estimation of age, particularly in cases where the dispersion in measured D_e values is
618 dominated by extrinsic over-dispersion rather than measurement uncertainties. This conclusion has
619 important implications for the analysis of more complicated dose distributions affected by incomplete
620 bleaching and post-depositional mixing.

621

622 **Acknowledgements**

623 This work was funded by a H.C. Ørsted postdoctoral grant awarded to GG. Monte Carlo simulations were
624 performed at the Calculation Centre of the French National Institute for Nuclear and Particle Physics
625 (CCIN2P3) via the TGE Adonis/TGIR Huma-Num. The authors are grateful to two anonymous reviewers
626 for constructive and useful comments on an earlier version of this article.

627 **References**

- 628 Agostinelli S., et al. (Geant4 Collaboration) (2003). Geant4 - a simulation toolkit. *Nuclear Instruments*
629 *and Methods A*, 506, 250-303.
- 630 Allison J., *et al.* (Geant4 Collaboration) (2006). Geant4 developments and applications. *IEEE Transactions*
631 *on Nuclear Sciences*, 53, 270-278.
- 632 Ankjærgaard, C., Murray, A.S., 2007. Total beta and gamma dose rates in trapped charge dating based
633 on beta counting. *Radiation Measurements* 42, 352-359.
- 634 Arnold, L. J., Roberts, R. G., Galbraith, R. F., DeLong, S. B., 2009. A revised burial dose estimation
635 procedure for optical dating of young and modern-age sediments. *Quaternary Geochronology* 4, 306-
636 325.
- 637 Blott, S.J., Pye, K., 2001. Gradistat: a grain size distribution and statistics package for the analysis of
638 unconsolidated sediments. *Earth Surface Processes and Landforms*, 26, 1237–1248.

639 Bos, A.J.J., Wallinga, J., Johns, C., Abellon, R.D., Brouwer, J.C., Schaart, D.R., Murray, A.S., 2006. Accurate
640 calibration of a laboratory beta particle dose rate for dating purposes. *Radiation Measurements*, 41,
641 1020-1025.

642 Brennan, B. J. 2006. Variation of the alpha dose rate to grains in heterogeneous sediments. *Radiation*
643 *Measurements* 41, 1026-1031.

644 Brennan, B. J., Schwarcz H. P., Rink J., 1997. Simulation of the gamma radiation field in lumpy
645 environments. *Radiation Measurements* 27, 2, 299-305.

646 Buylaert, J.-P., Ankjaergaard, C., Murray, A.S., Nielsen, A., 2006. A proposed laboratory intercomparison
647 sample based on a beach-ridge sand from Skagen (Denmark), poster. In: UK-LED Meeting, Liverpool.

648 Buylaert, J-P, Thiel, C, Murray, A.S., Vandenberghe, D.A.G., Yi, S., Lu, H., 2011. IRSL and post-IR IRSL
649 residual doses recorded in modern dust samples from the Chinese Loess Plateau. *Geochronometria*, 38,
650 432-440.

651 Bøtter-Jensen, L., Bulur, E., Duller, G.A.T., Murray, A.S., 2000. Advances in luminescence instrument
652 systems. *Radiation Measurements* 32, 523–528.

653 Bøtter-Jensen, L., Andersen, C.E., Duller, G.A.T., Murray, A.S., 2003. Developments in radiation,
654 stimulation and observation facilities in luminescence measurements. *Radiation Measurements* 37, 535–
655 541.

656 Bøtter-Jensen, L., Thomsen, K.J., Jain, M., 2010. Review of optically stimulated luminescence (OSL)
657 instrumental developments for retrospective dosimetry. *Radiation Measurements*, 45, 253-257.

658 Chauhan, N., Singhvi, A., 2011. Distribution in SAR palaeodoses due to spatial heterogeneity of natural
659 beta dose. *Geochronometria*, 38, 190-198.

660 Cunningham, A. C., DeVries, D. J., Schaart, D. R., 2012. Experimental and computational simulation of
661 beta-dose heterogeneity in sediment. *Radiation Measurements*, 47, 1060-1067.

662 Donev A., Stillinger F. H., Torquato S., 2005. Neighbor List Collision-Driven Molecular Dynamics
663 Simulation for Nonspherical Particles. I. Algorithmic Details II. Applications to Ellipses and Ellipsoids,
664 *Journal of Computational Physics*, 202(2), 737-764 (part I) and 765-793 (part II).

665 Duller, G.A.T., Bøtter-Jensen, L., Murray, A.S., Truscott, A.J., 1999. Single grain laser luminescence (SGLL)
666 measurements using a novel automated reader. *Nuclear Instruments and Methods B*, 155, 506–514.

667 Folk, R.L., Ward, W.C., 1957. Brazos River bar: a study in the significance of grain size parameters.
668 *Journal of Sedimentary Petrology*, 27, 3-26.

669 Galbraith, R. F., Green, P. F., 1990. Estimating the component ages in a finite mixture. *Nuclear Tracks*
670 *and Radiation Measurements* 17, 196-206.

671 Galbraith, R.F., Roberts, R.G., 2012. Statistical aspects of equivalent dose and error calculation and
672 display in OSL dating: an overview and some recommendations. *Quaternary Geochronology* 11, 1-27.

673 Galbraith, R., Roberts, R.G., Laslette, G., Yoshida, H., Olley, J., 1999. Optical dating of single and
674 multiple grain quartz from Jinmium rock shelter, northern Australia. Part I. Experimental design and
675 statistical models R.F. *Archaeometry* 41, 339-364.

676 Galbraith, R.F., Roberts, R.G., Yoshida, H., 2005. Error variation in OSL palaeodose estimates from single
677 aliquots of quartz: a factorial experiment. *Radiation Measurements* 39, 289-307.

678 Guérin, 2011. Modélisation et simulation des effets dosimétriques dans les sédiments quaternaires :
679 application aux méthodes de datation par luminescence. PhD thesis. Université Bordeaux 3.

680 Guérin, G., Mercier, N. and Adamiec, G., 2011. Dose rate conversion factors: update. *Ancient TL*, 29 (1),
681 5-8.

682 Guérin, G., Mercier, N., 2012. Preliminary insight into dose deposition processes in sedimentary media
683 on a grain scale: Monte Carlo modelling of the effect of water on gamma dose rates. *Radiation*
684 *Measurements*, 47, 541-547.

685 Guérin, G., Mercier, N., Nathan R., Adamiec, G., Lefrais, Y., 2012. On the use of the infinite matrix
686 assumption and associated concepts: a critical review. *Radiation Measurements*, 47, 778-785.

687 Guérin, G., Murray A. S., Jain M., Thomsen K. J., Mercier, N., 2013. How confident are we in the
688 chronology of the transition between Howieson's Poort and Still Bay? *Journal of Human Evolution* 64,
689 314-317.

690 Huntley D.J., Lamothe M., 2001. Ubiquity of anomalous fading in K-feldspar and the measurement and
691 correction for it in optical dating. *Canadian Journal of Earth Sciences* 38, 1093–1106.

692 Jacobs Z., 2010. An OSL chronology for the sedimentary deposits from Pinnacle Point Cave 13B—A
693 punctuated presence. *Journal of Human Evolution* 59, 289-305.

694 Jacobs, Z., Roberts, R.G., Galbraith, R.F., Deacon, H.J., Grün, R., Mackay, A., Mitchell, P., Vogelsang, R.,
695 Wadley, L., 2008a. Ages for the Middle Stone Age of southern Africa: implications for human behavior
696 and dispersal. *Science* 322, 733-735.

697 Jacobs, Z., Wintle, A.G., Roberts, R.G., Duller, G.A.T., 2008b. Equivalent dose distributions from single
698 grains of quartz at Sibudu, South Africa: context, causes and consequences for optical dating of
699 archaeological deposits. *Journal of Archaeological Science* 35, 1808-1820.

700 Jacobs, Z., Meyer, M.C., Roberts, R.G., Aldeais, V., Dibble, H., El Hajraoui, M.A., 2011. Single-grain OSL
701 dating at La Grotte des Contrebandiers ('Smugglers' Cave'), Morocco: improved age constraints for the
702 Middle Paleolithic levels. *Journal of Archaeological Science* 38, 3631-3643.

703 Jacobs, Z., Roberts, R.G., Nespoulet, R., El Hajraoui, M.A., Debénath, A., 2012. Single grain OSL
704 chronologies for Middle Palaeolithic deposits at El Mnasra and El Harhoura 2, Morocco: implications for
705 Late Pleistocene human-environment interactions along the Atlantic coast of northwest Africa. *Journal*
706 *of Human Evolution* 62, 377-394.

707 Jacobs, Z., Hayes E. H., Roberts, R.G., Galbraith, R. F., Henshilwood, C.S., 2013. An improved OSL
708 chronology for the Still Bay layers at Blombos Cave, South Africa: further tests of single-grain dating
709 procedures and a re-evaluation of the timing of the Still Bay industry across southern Africa. *Journal of*
710 *Archaeological Science* 40, 579-594.

711 Jain, M., Thomsen, K.J., Bøtter-Jensen, L., Murray, A.S., 2004. Thermal transfer and apparent-dose
712 distributions in poorly bleached mortar samples: results from single grains and small aliquots. *Radiation*
713 *Measurements* 38, 101-109.

714 Lapp, T., Jain, M., Thomsen, K. J., Murray, A. S. & Buylaert, J. P., 2012. New luminescence measurement
715 facilities in retrospective dosimetry. *Radiation Measurements* 47, 803–808.

716 Lepper, K., 2001. Development of an objective dose distribution analysis method for OSL dating and pilot
717 studies for planetary applications. Ph.D. Thesis, Oklahoma State University, Stillwater.

718 Mayya, Y.S., Morthekai, P., Murari, M.K., Singhvi, A.K., 2006. Towards quantifying beta microdosimetric
719 effects in single-grain quartz dose distribution. *Radiation Measurements*, 41, 1032-1039.

720 Murray, A. S., Wintle, A. G., 2000. Luminescence dating of quartz using an improved single-aliquot
721 regenerative-dose protocol. *Radiation Measurements* 32, 57-73.

722 Murray, A. S., Wintle, A. G., 2003. The single aliquot regenerative dose protocol: potential for
723 improvements in reliability. *Radiation Measurements* 37, 377-381.

724 Murray, A.S., Thomsen, K.J., Masuda, N., Buylaert, J.P., Jain, M., 2012. Identifying well-bleached quartz
725 using the different bleaching rates of quartz and feldspar luminescence signals. *Radiation*
726 *Measurements* 47, 688-695.

727 Nathan R. P., 2011. Numerical modelling of the environmental dose rate for trapped charge dating.
728 Unpublished PhD thesis, University of Oxford.

729 Nathan R.P, Mauz B., 2008. On the dose rate estimate of carbonate-rich sediments for trapped charge
730 dating. *Radiation Measurements* 43, 14-25.

731 Nathan, R.P., Thomas, P.J., Jain, M., Murray, A.S., Rhodes, E.J., 2003. Environmental dose rate
732 heterogeneity of beta radiation and its implications for luminescence dating: Monte Carlo modelling and
733 experimental validation. *Radiation Measurements* 37, 305-313.

734 Nielsen, A., Murray, A.S., Pejrup, M., Elberling, B., 2006. Optically stimulated luminescence dating of a
735 Holocene beach ridge plain in northern Jutland, Denmark. *Quaternary Geochronology* 1 (4), 305-312.

736 Olley, J.M., De Deckker, P., Roberts, R.G., Fifield, L.K., Yoshida, H., Hancock, G., 2004. Optical dating of
737 deep-sea sediments using single grains of quartz: a comparison with radiocarbon. *Sedimentary Geology*
738 169, 175-189.

739 Roberts, R.G., Galbraith, R.F., Yoshida, H., Laslett, G.M., Olley, J.M., 2000. Distinguishing dose
740 populations in sediment mixtures: a test of single-grain optical dating procedures using mixtures of
741 laboratory-dosed quartz. *Radiation Measurements* 32, 459-465.

742 Salvat F., Fernández-Varea, J.M. and Sempau, J., 2011. PENELOPE-2011: A Code System for Monte Carlo
743 Simulation of Electron and Photon Transport OECD NEA Data Bank/NSC DOC(2011)/5 (OECD Nuclear
744 Energy Agency, Issy-les-Moulineaux, 2011).

745 Salvat, F., Fernandez-Varea, J.M., Acosta, E., Sempau, J., 2011. PENELOPE - A Code System for Monte
746 Carlo Simulation of Electron and Photon Transport. Workshop Proceedings, Issy-les-Moulineaux, France,
747 (November 2001), AEN-NEA.

748 Singhvi, A.K., Stokes, S.C., Chauhan, N., Nagar, Y.C., Jaiswal, M.K., 2011. Changes in natural OSL
749 sensitivity during single aliquot regeneration procedure and their implications for equivalent dose
750 determination. *Geochronometria* 38, 231-241.

751 Stokes, S., 1994a. The timing of OSL sensitivity changes in a natural quartz. *Radiation Measurements* 23,
752 601-605.

753 Stokes, S., 1994b. Optical Dating of selected late Quaternary aeolian sediments from the south western
754 United States. Unpublished D. Phil. thesis. Oxford University.

755 Thiel, C., Buylaert, J.P., Murray, A., Terhorst, B., Hofer, I., Tsukamoto, S., Frechen, M., 2011.
756 Luminescence dating of the Stratzing loess profile (Austria) - testing the potential of an elevated
757 temperature post-IR IRSL protocol. *Quaternary International*, 234, 23-31.

758 Thomsen, K.J., Murray, A.S., Bøtter-Jensen, L., 2005. Sources of variability in OSL dose measurements
759 using single grains of quartz. *Radiation Measurements*, 39, 47-61.

760 Thomsen, K.J., Murray, A.S., Bøtter-Jensen, L., Kinahan, J., 2007. Determination of burial dose in
761 incompletely bleached fluvial samples using single grains of quartz. *Radiation Measurements* 42 (3), 370-
762 379.

763 Thomsen K. J., Murray A. S., Jain M., 2012. The dose dependency of the over-dispersion of quartz OSL
764 single grain dose distributions. *Radiation Measurements* 47, 732-739.

765 Tribolo, C., Mercier, N., Rasse, M., Soriano, S., Huysecom, E., 2010. Kobo 1 and L'Abri-aux-Vaches (Mali,
766 West Africa): two cases study for the optical dating of bio-turbated sediments. *Quaternary*
767 *Geochronology* 5, 317-323.

768

769 **Figure captions**

770 Fig. 1: example of a Geant4 simulation of beta emission from potassium feldspars. The grains are
771 randomly packed using the LSD algorithm (Donev *et al.*, 2005). Blue spheres represent potassium-rich
772 feldspar grains, whereas grey ones represent quartz grains. Electron tracks generated inside feldspar
773 grains are shown in red, while secondary photon tracks are shown in green.

774 Fig. 2: single grain OSL natural test dose response as a function of dose for (a) Risø calibration quartz
775 (annealed by heating and then given a 4.81 Gy gamma dose), quartz from the intercomparison sample
776 bleached in a daylight simulator (Hönle SOL 2) at a distance of 80 cm for 3 hours and then given gamma
777 doses of 1.92 Gy (b), 4.81 Gy (c) and 9.62 Gy (d), and natural (e).

778 Fig. 3: Q-Q plots of the standardised residuals from CAM_{UL} (left) and CAM (right). Risø calibration quartz
779 (a); quartz from the intercomparison sample: bleached and given gamma doses of 1.92 Gy (b), 4.81 Gy
780 (c) and 9.62 Gy (d).

781 Fig. 4: Geant4-simulated beta dose rate distribution from potassium-rich feldspar grains to single grains
782 of quartz in the intercomparison sample.

783 Fig. 5: Q-Q plots of the standardised residuals from CAM_{UL} (left) and CAM (right), for the natural D_e
784 distribution from the intercomparison sample.

785 Fig. 6: The different grain size distributions simulated with Geant4, corresponding to well-sorted sands.
786 While the shape of the distributions is unchanged, the grain sizes are multiplied by different factors to
787 investigate the effect of mean grain size on the single-grain dose rate distributions. The shaded bar
788 indicates the 180-250 µm fraction, from which each grain is treated as an independent dosimeter.

789 Fig. 7: Examples of beta dose rate distributions from potassium feldspar in well-sorted sands for
790 different potassium contents and mean grain sizes. The relative standard deviation is indicated in each
791 case (RSD). Left: the potassium content is fixed (1.10%) but the mean grain size increases from top to
792 bottom. Right: the mean grain size is fixed (360 µm) but the potassium content increases from top to
793 bottom.

794 Fig. 8: Relative standard deviation, obtained with Geant4 simulations, of single grain beta dose rate
795 distributions from potassium, as a function of potassium content for different grain sizes.

796 Fig. 9: Relative standard deviation, obtained with Geant4 simulations, of total dose rates to single grains
797 of quartz, as a function of potassium content for different grain sizes. Total dose rate is 1 Gy.ka⁻¹ (a), 2
798 Gy.ka⁻¹ (b), 3 Gy.ka⁻¹ (c). The dashed lines indicate the range of most likely values for potassium content
799 in each case (see text for details).

800 Fig. 10: Single grain OSL absolute (left) and relative (right) uncertainties as a function of dose. (a), (b):
801 intercomparison sample, 4.81 Gy gamma distribution. (c), (d): intercomparison sample, natural
802 distribution. Inset in (c): without the 3 high uncertainty points.

K (%)	U (ppm)	Th (ppm)	Water content (%)	Gamma dose-rate (Gy.ka ⁻¹)	Beta dose-rate (Gy.ka ⁻¹)	Cosmic (Gy.ka ⁻¹)	Total (Gy.ka ⁻¹)	Fraction contributed by beta from K
1.06 ± 0.02	0.42 ± 0.02	1.38 ± 0.04	12	0.33 ± 0.01	0.74 ± 0.03	0.17	1.24 ± 0.06	0.50

Table 1: Radiometric and dose-rate data for the inter-comparison sample, as measured in IRAMAT-CRP2A.

Quartz OSL		Feldspar IRSL at 50 °C		Feldspar postIR-IRSL at 290 °C	
D _e (Gy)	Age (ka)	D _e (Gy)	Age (ka) ^a	D _e (Gy)	Age (ka)
4.73 ± 0.23	3.81 ± 0.26	6.90 ± 0.30	4.28 ± 0.27	13.7 ± 0.6	6.69 ± 0.36

Table 2: Ages obtained for the intercomparison sample, using quartz OSL, feldspar IRSL at 50 °C and post-IR IRSL at 290 °C.

^a the Huntley and Lamothe fading correction model was applied.

	Given dose (Gy)	n ^b	Avg. error (%) ^c	CAM			CAM-UL				Unweighted average	
				De (Gy)	OD (%)	Recovery ratio	De (Gy)	OD (Gy)	OD (% of D _e)	Recovery ratio	De (Gy)	Recovery ratio
InterComp.	1.92 ± 0.03	85	27	1.86 ± 0.06	17 ± 3	0.97 ± 0.03	1.79 ± 0.07	0.35 ± 0.05	0.20	0.93 ± 0.03	1.88 ± 0.08	0.98 ± 0.04
	4.81 ± 0.07	71	21	4.74 ± 0.16	15 ± 3	0.98 ± 0.03	4.58 ± 0.17	0.88 ± 0.12	0.19	0.95 ± 0.03	4.63 ± 0.12	0.96 ± 0.02
	9.62 ± 0.14	108	13	9.63 ± 0.28	15 ± 2	1.00 ± 0.02	9.49 ± 0.28	1.5 ± 0.2	0.16	0.99 ± 0.02	9.81 ± 0.33	1.02 ± 0.03
	Nat	123	23	4.51 ± 0.15	23 ± 2		4.38 ± 0.16	1.2 ± 0.1	0.28		4.56 ± 0.19	
Risø Cal. ^a	4.81 ± 0.07	369	13	108 ± 1	15 ± 1		106 ± 1	18 ± 1	0.17		108 ± 1	

Table 3: Statistics of the different single-grain quartz D_e distributions.

^a for the Risø calibration quartz, all measured equivalent doses are given in seconds rather than in Gy, as the result is used for dose-rate calibration of the reader.

^b Number of accepted grains.

^c Average relative uncertainty on individual dose estimates.

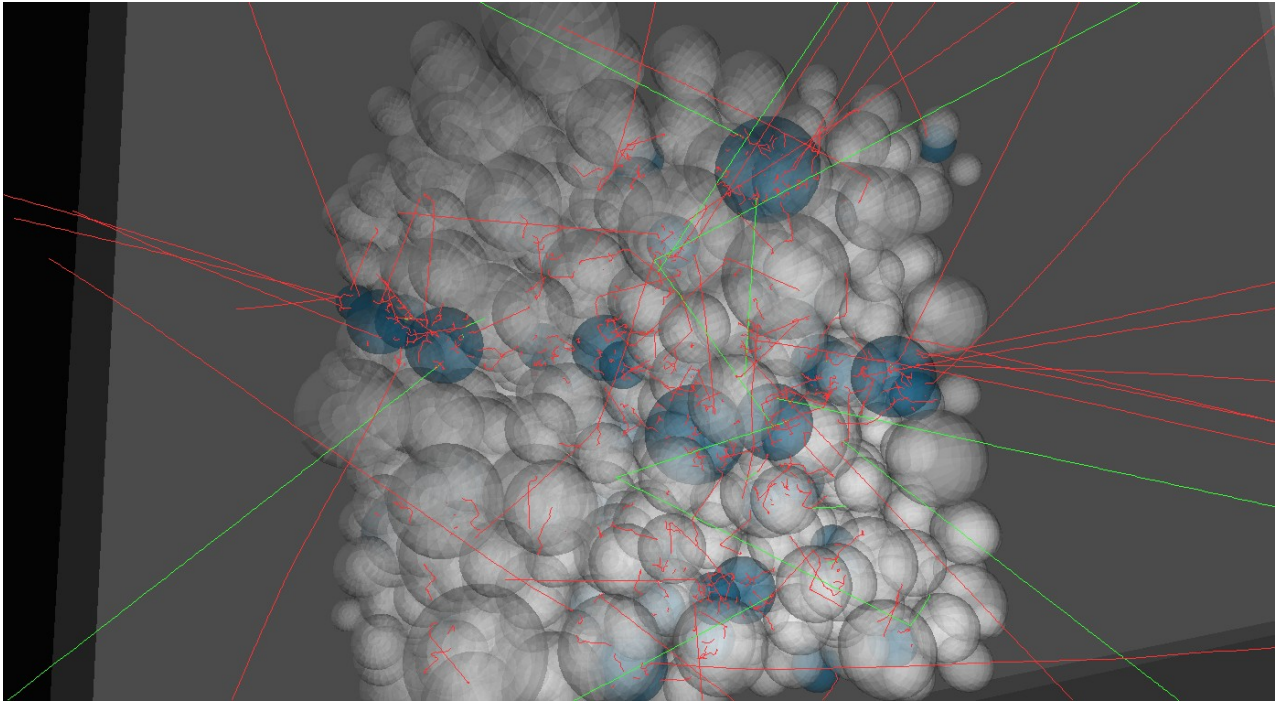


Fig. 1

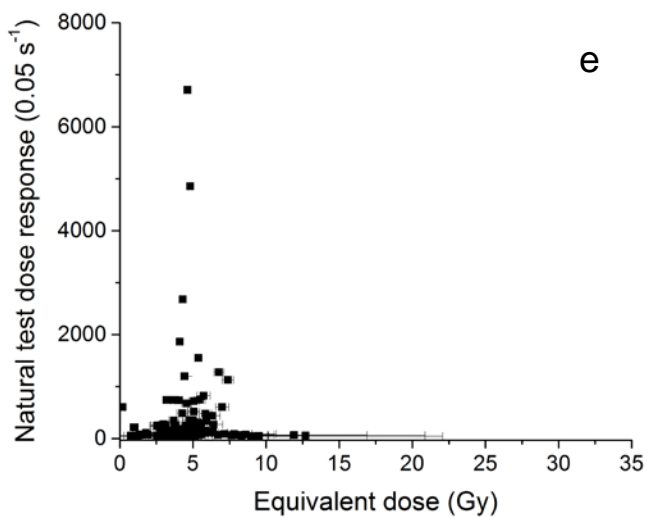
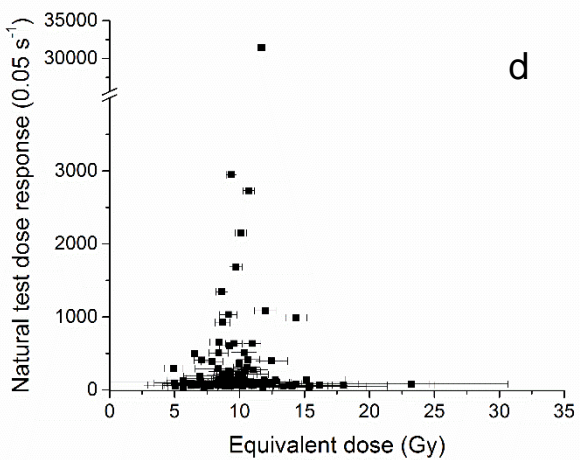
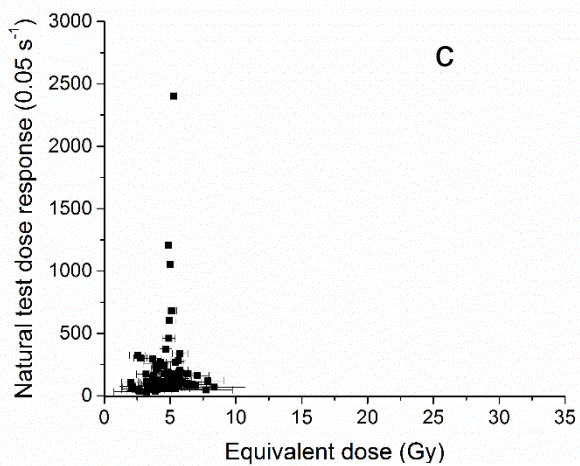
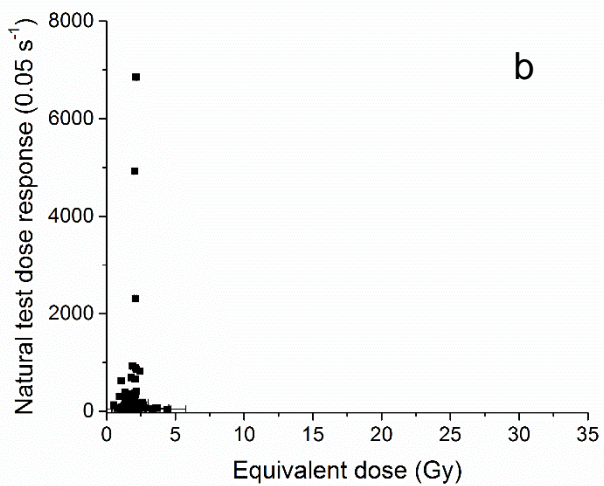
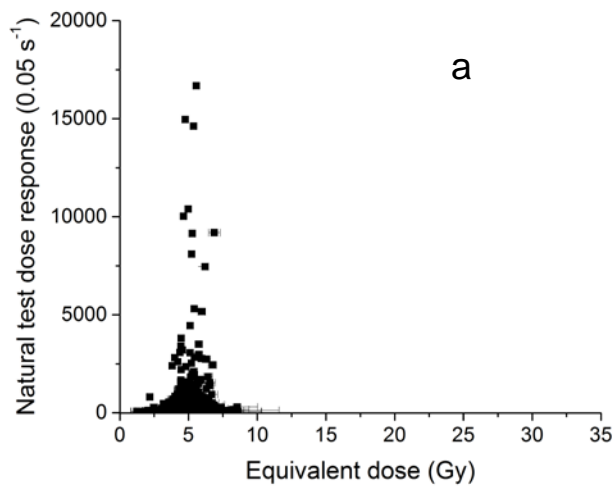
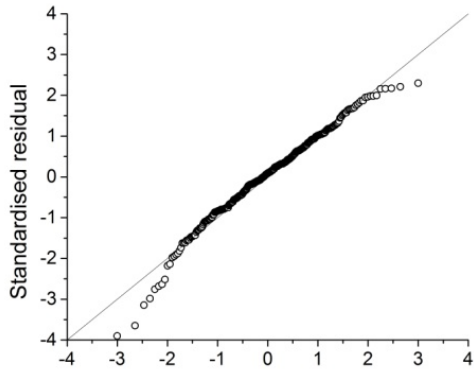
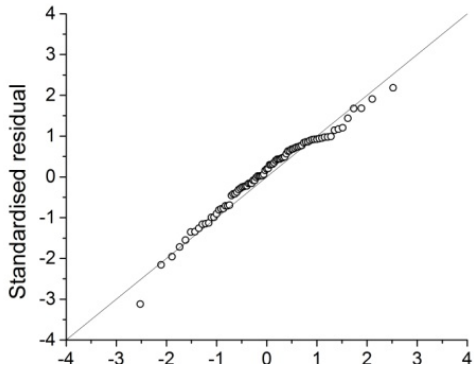
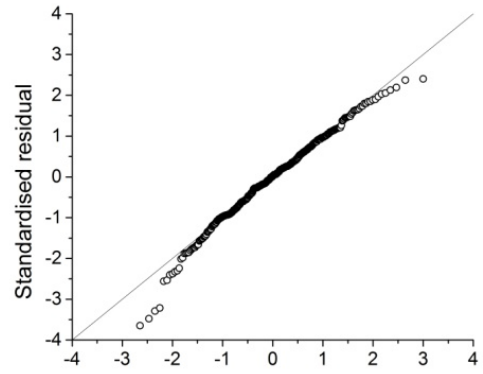


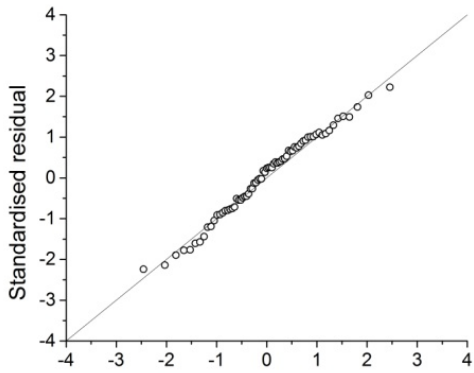
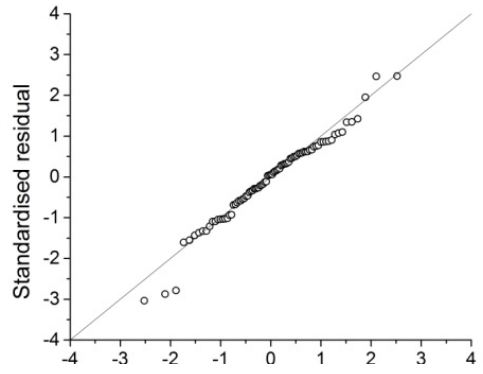
Fig. 2:



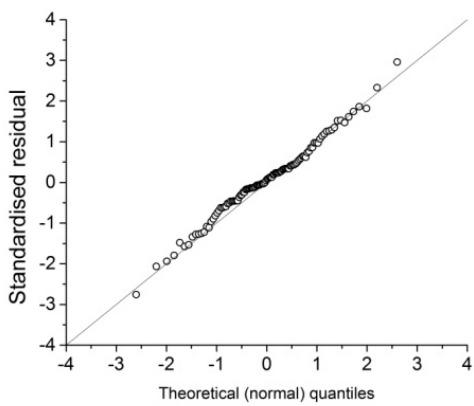
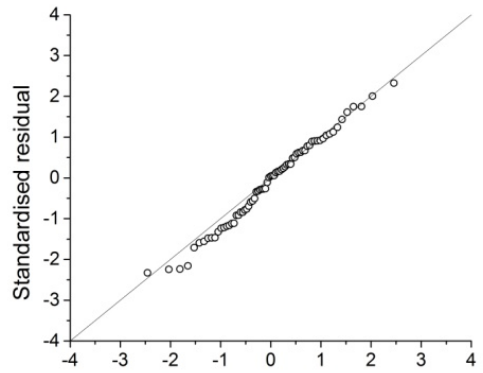
a



b



c



d

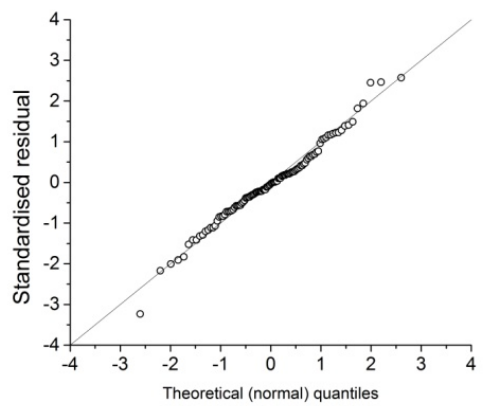


Fig. 3:

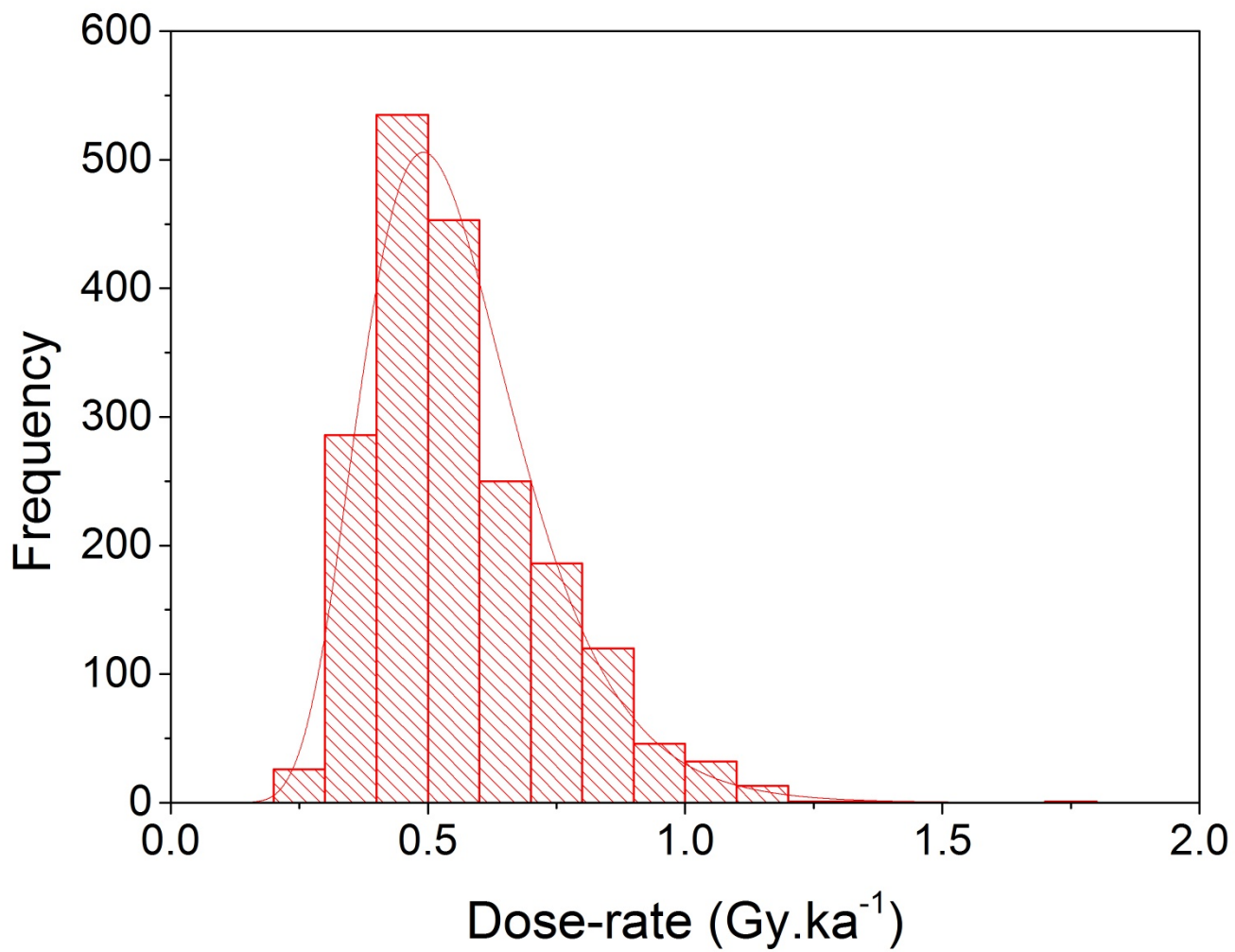


Fig. 4:

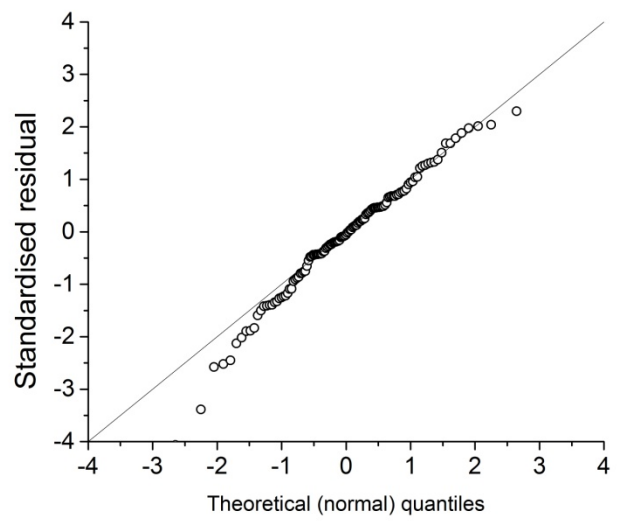
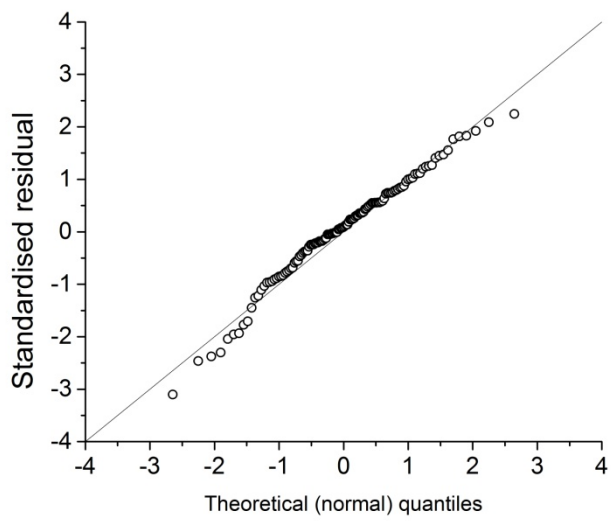


Fig. 5:

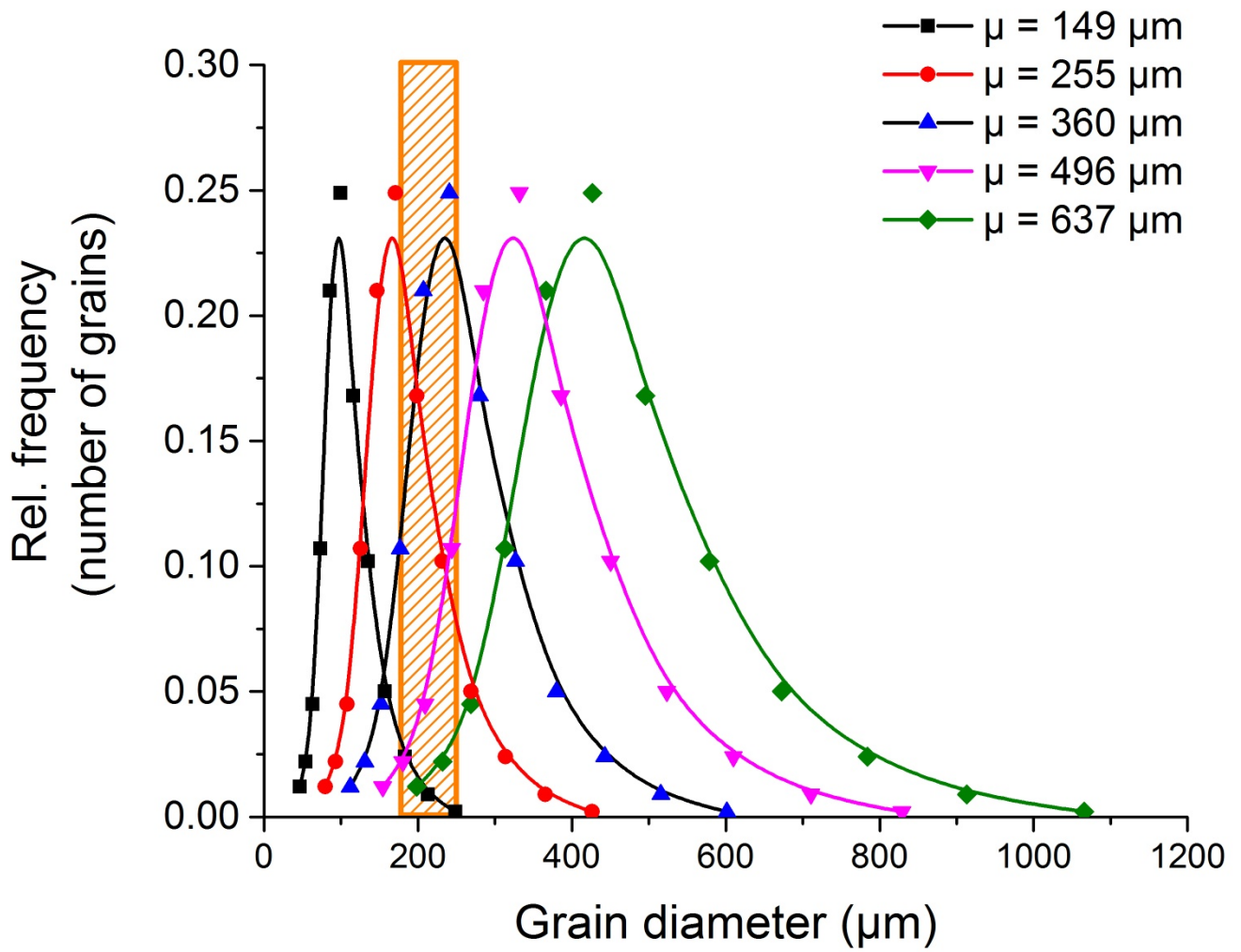


Fig. 6:

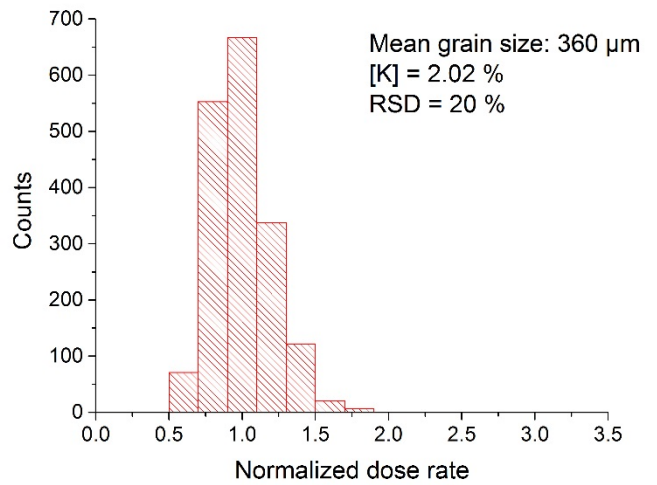
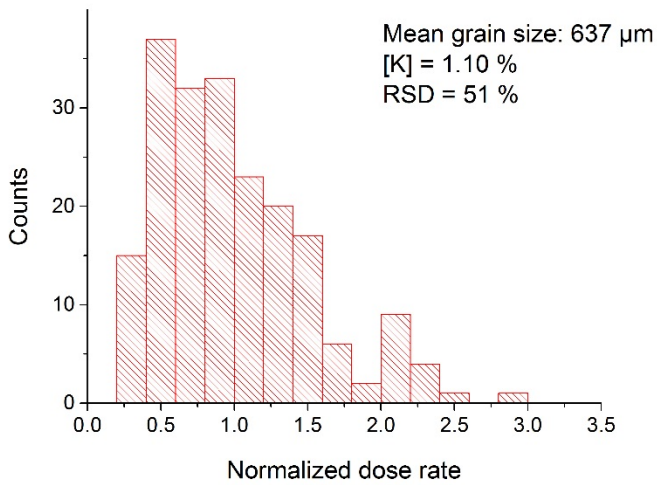
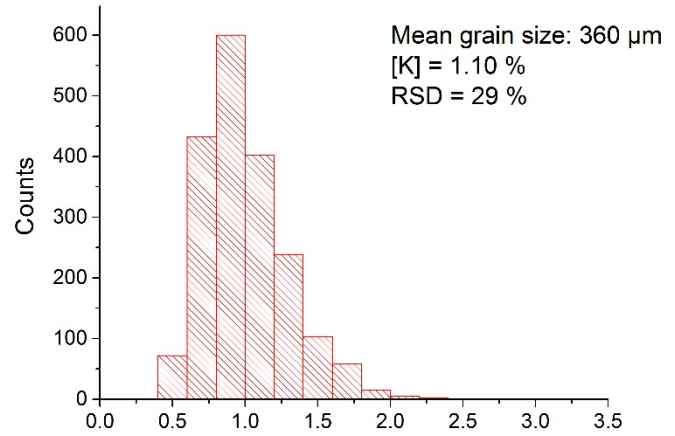
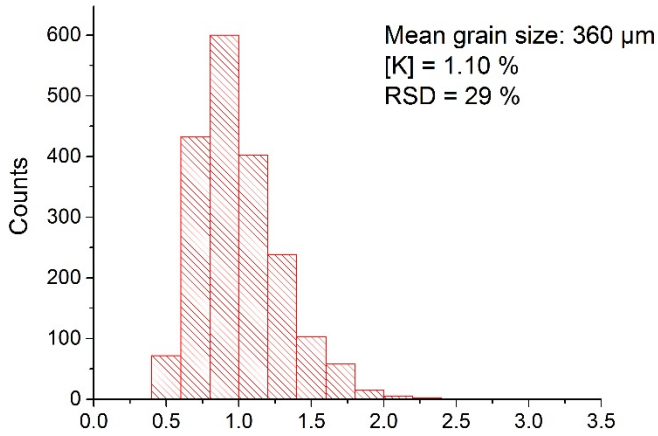
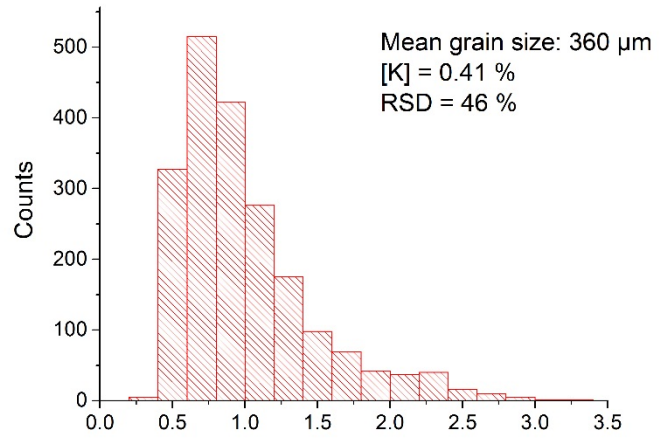
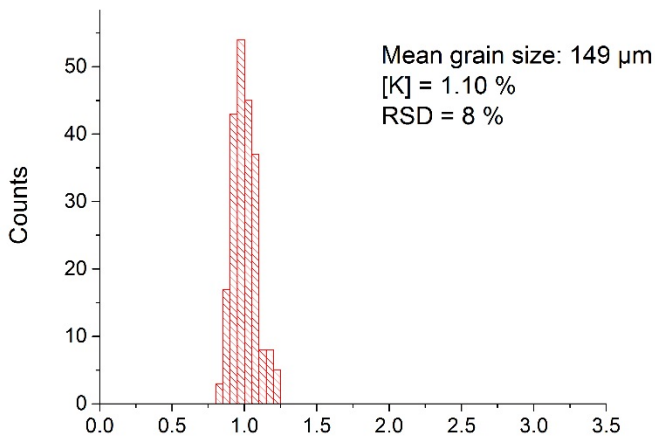


Fig. 7

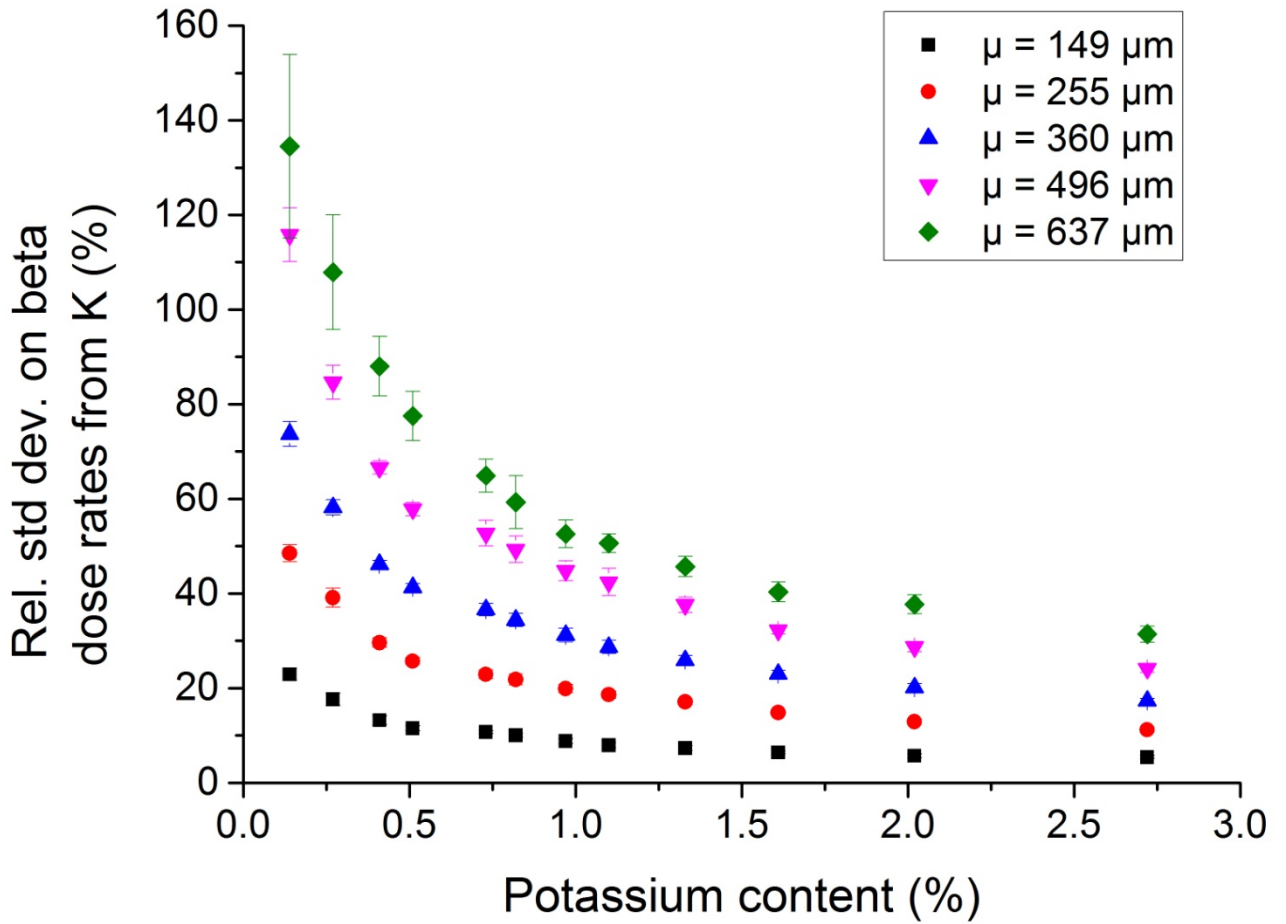


Fig. 8

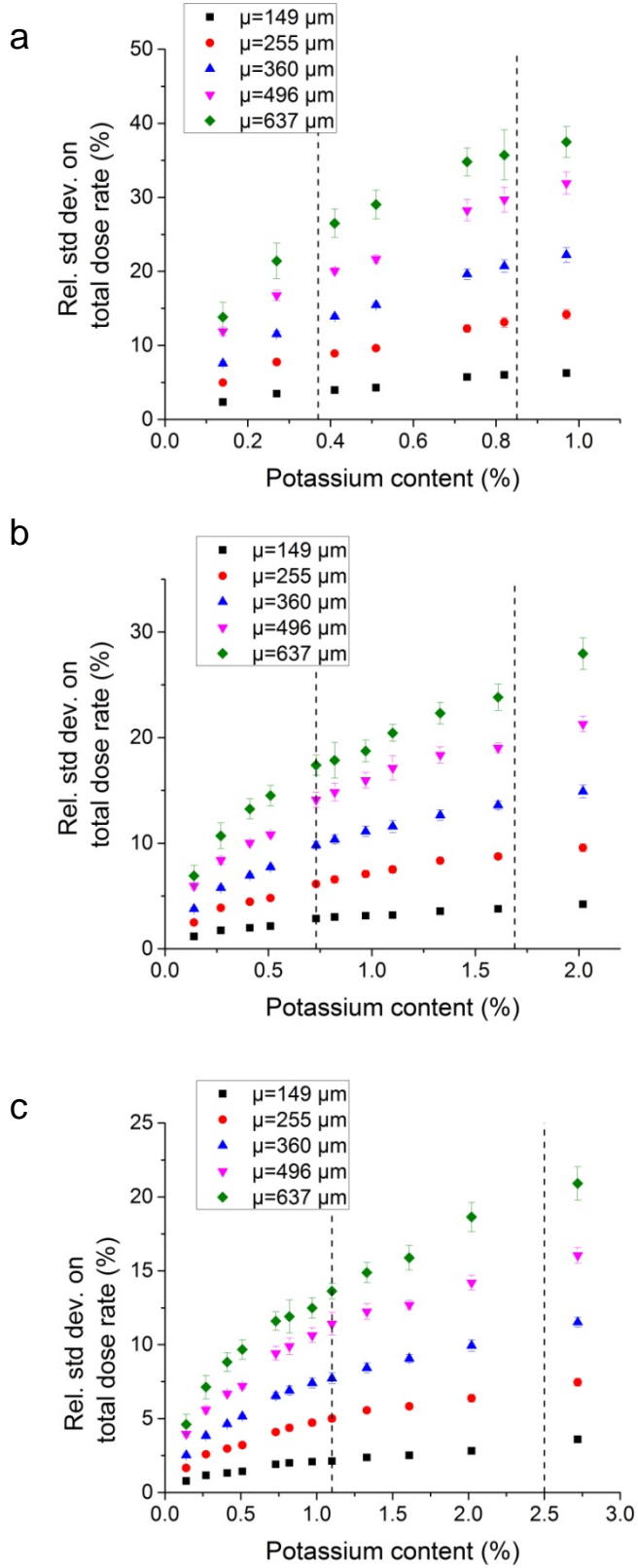


Fig. 9

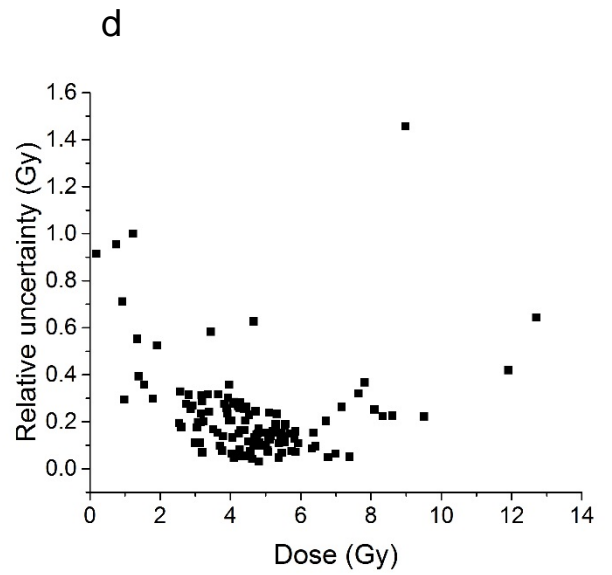
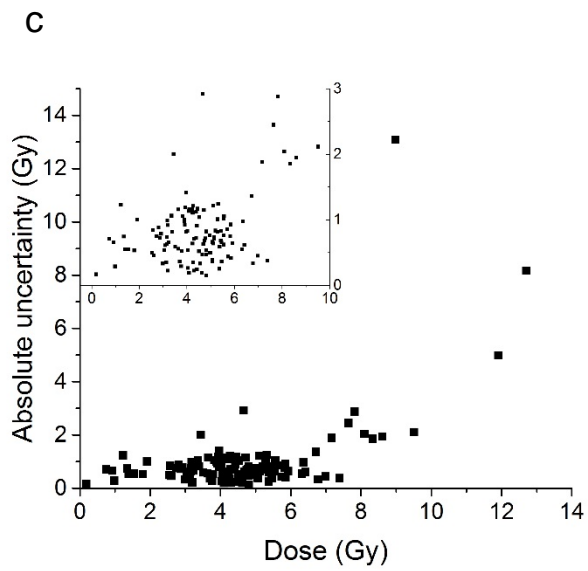
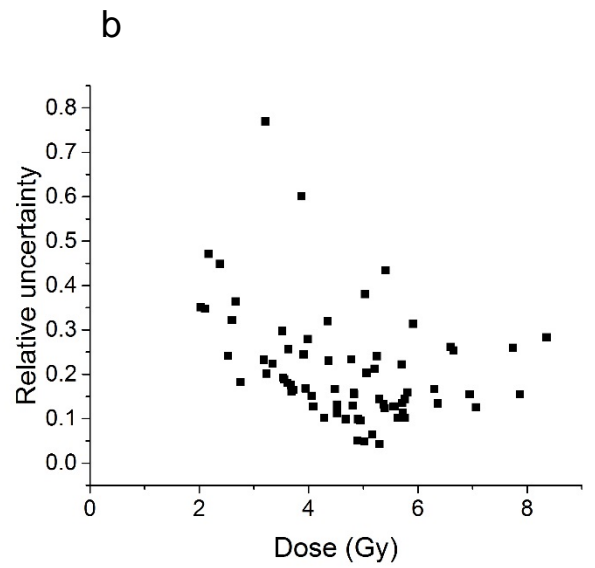
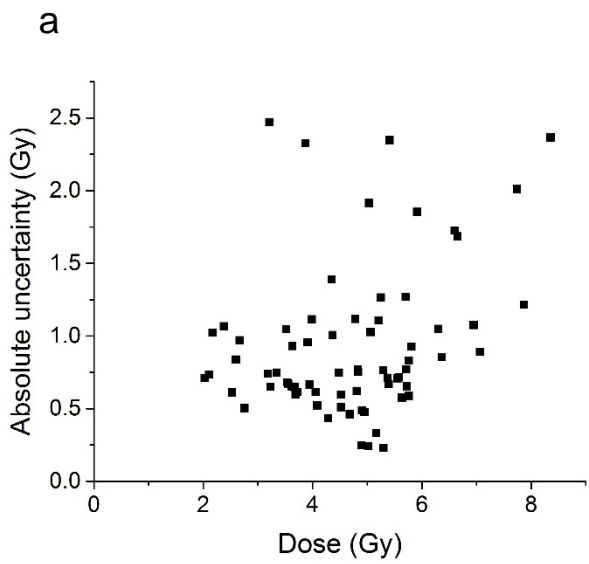


Fig. 10